An epigenetically distinct HSC subset supports thymic reconstitution

Harold K. Elias[1,2], Sneha Mitra[3], Marina B. da Silva[1,14], Adhithi Rajagopalan[1,14], Brianna Gipson[1], Nicole Lee[1], Anastasia I. Kousa[1], Mohamed A.E. Ali[4], Simon Grassman[1], Xiaoqun Zhang[1], Susan DeWolf [6], Melody Smith[5], Hana Andrlova[1], Kimon V. Argyropoulos[1], Roshan Sharma[7], Teng Fei[8], Joseph C Sun[1], Cynthia E. Dunbar[9], Christopher Y Park[4], Christina S. Leslie[3], Avinash Bhandoola[10], and Marcel R.M. van den Brink[1,11,12,13]

Affiliations

[1]Department of Immunology, Sloan Kettering Institute, Memorial Sloan Kettering Cancer Center, New York, NY, 10065, USA

[2]National Institutes of Health (NIH), Bethesda, MD, 20892, USA, USA

[3]Computational and Systems Biology, Sloan Kettering Institute, Memorial Sloan Kettering Cancer Center, New York, NY, 10065, USA

[4]Department of Pathology, New York University Grossman School of Medicine, New York, NY, 10016, USA

[5]Division of Blood and Marrow Transplantation and Cellular Therapy, Department of Medicine, Stanford University School of Medicine, Stanford, CA, 94305

[6]Leukemia Service, Department of Medicine, Memorial Sloan Kettering Cancer Center, New York, NY, 10065, USA

[7]Single-cell Analytics and Innovation Lab, Sloan Kettering Institute, Memorial Sloan Kettering Cancer Center, New York, NY, 10065, USA

[8]Department of Epidemiology and Biostatistics, Memorial Sloan Kettering Cancer Center, New York, NY, 10065, USA

[9]Translational Stem Cell Biology Branch, National Heart, Lung, and Blood Institute, NIH, Bethesda, MD, 20892, USA

[10]Laboratory of Genome Integrity, Center for Cancer Research, National Cancer Institute, NIH, Bethesda, MD, 20892, USA

[11]Department of Immunology and Microbial Pathogenesis, Weill Cornell Medical College; New York, NY

[12]Department of Medicine, Memorial Sloan Kettering Cancer Center, New York, NY, 10065, USA.

[13]Lead Contact

[14]These authors contributed equally

Correspondence: eliash@mskcc.org (HKE); mvandenbrink@coh.org (MRMvdB)

ABSTRACT

Hematopoietic stem cells (HSCs) with multilineage potential are critical for effective T cell reconstitution and restoration of the adaptive immune system after allogeneic Hematopoietic Cell Transplantation (allo-HCT). The Kit^{lo} subset of HSCs is enriched for multipotential precursors,[1, 2] but their T-cell lineage potential has not been well-characterized. We therefore studied the thymic reconstituting and T-cell potential of Kit^{lo} HSCs. Using a preclinical allo-HCT model, we demonstrate that Kit^{lo} HSCs support better thymic recovery, and T-cell reconstitution resulting in improved T cell responses to infection post-HCT. Furthermore, Kit^{lo} HSCs with augmented BM lymphopoiesis mitigate age-associated thymic alterations, thus enhancing T-cell recovery in middle-aged hosts. We find the frequency of the Kit^{lo} subset declines with age, providing one explanation for the reduced frequency of T-competent HSCs and reduced T-lymphopoietic potential in BM precursors of aged mice.[3, 4, 5] Chromatin profiling revealed that Kit^{lo} HSCs exhibit higher activity of lymphoid-specifying transcription factors (TFs), including *Zbtb1*. Deletion of *Zbtb1* in Kit^{lo} HSCs diminished their T-cell potential, while reinstating *Zbtb1* in megakaryocytic-biased Kit^{hi} HSCs rescued T-cell potential, *in vitro* and *in vivo*. Finally, we discover an analogous Kit^{lo} HSC subset with enhanced lymphoid potential in human bone marrow. Our results demonstrate that Kit^{lo} HSCs with enhanced lymphoid potential have a distinct underlying epigenetic program.

KEYWORDS: Hematopoietic stem cells; lymphoid differentiation; epigenetic priming; thymus; immune reconstitution; immunosenescence.

INTRODUCTION

T lymphocytes play a crucial role in the adaptive immune response. A highly diverse T cell pool is required to recognize and eliminate foreign pathogens while also maintaining self-tolerance. The thymus continuously produces T cells, but with advancing age, its regenerative capacity declines,[6] leading to decreased thymic output and compromised T cell diversity. Furthermore, the thymus is also vulnerable to acute damage from infections, cancer therapies, and conditioning regimens for allogeneic hematopoietic cell transplantation (allo-HCT), which results in prolonged T cell lymphopenia, thereby increasing the risk of infections and cancer relapse, contributing to transplant-related complications and mortality.[7] Likely for these reasons, early T-cell reconstitution is a positive prognostic indicator of allo-HCT outcomes.[8, 9]

Post-transplant T cell reconstitution requires a steady supply of hematopoietic stem cells (HSCs)-derived lymphoid progenitors[10] as well as thymic recovery. Prior research has demonstrated that thymic integrity is dependent on thymocyte-stromal crosstalk, particularly in the thymic epithelial cell (TEC) compartment.[11, 12, 13] Age-associated reduced lymphoid potential originating at the level of HSCs,[14] coupled with thymic decline[6] contribute to delayed immune recovery. Therefore, identifying strategies to augment T lymphopoiesis and promote thymic regeneration is an unmet clinical need.

Single-cell transplantation with tracking and sequencing of progeny[15, 16, 17, 18, 19, 20] has uncovered heterogeneity in self renewal capacity as well as lineage output among reconstituting HSCs-highlighting HSCs with multilineage versus lineage-biased potential. These studies showed that, while only a fraction of HSCs generate “balanced” multilineage output, the majority exhibit a diverse range of lineage potential following transplantation- varying in their contributions and reconstitution kinetics for each lineage, thereby showcasing their inherent biases. These lineage

biases are intrinsically stable and maintained following transplantation.[21, 22, 23] At the molecular level, these cell autonomous features are mediated by epigenetic configuration and are divergent from their transcriptional state.[18, 24] Although this suggests the existence of a highly organized and predictable framework for lineage-restricted fates of long-term self-renewing HSCs, the molecular identities, gene regulatory networks and functional implications of these differences governing lymphoid fate decisions remain largely unexplored.

Kit^{lo} HSCs have previously been described to exhibit better self-renewal and multipotency, including improved T-cell reconstitution in syngeneic transplant models. [1, 2]However, their thymic reconstituting ability, age-related changes, as well as the molecular basis for their enhanced T-cell lymphoid potential are unknown. Here, we delineate the pivotal role of Kit^{lo} HSCs in orchestrating thymic regeneration and immune reconstitution in both young and aged hosts. We find the frequency of the Kit^{lo} subset declines with age. Leveraging integrated single cell transcriptional and epigenetic profiling, we uncover the distinct epigenetic signature of Kit^{lo} HSCs, highlighting the presence of lymphoid-specifying transcription factor *Zbtb1* and its role in enhancing T-cell lymphoid potential. Additionally, we identify an analogous HSC subset in human bone marrow and demonstrate their enhanced lymphoid potential.

RESULTS

Reduced lymphoid output in aged HSCs impairs thymic recovery

Previous studies have shown impaired lymphoid reconstitution with aged HSCs in a syngeneic transplant model, yet this has not been explored using an allogeneic setting. We used a pre-clinical allo-HCT model to analyze immune reconstitution of young and old donors. To evaluate if HSCs with differences in lymphoid progenitor production could impact thymic recovery, we

transplanted Lin−Sca-1+Kit+ (LSK) CD34−CD150+CD48− cells LT-HSCs from young adult (2-mo) or old (24-mo) C57BL/6 mice with rescue BM cells (CD45.1) into lethally irradiated young BALB/cJ recipients (**Figure S1A**). Because HSC-derived thymic progeny emerge within 5-6 weeks,[25] we established an 8-week harvest timepoint. This interval allowed sufficient time for HSC-derived progenitors to repopulate the thymus, thereby providing a better understanding of thymic regeneration dynamics and the efficacy of HSC transplantation in promoting thymic reconstitution.

Consistent with prior reports, eight weeks post-HCT, we found that young HSCs supported balanced lineage reconstitution, while old HSCs exhibited significantly impaired T-cell reconstitution in the peripheral blood (PB), despite comparable reconstitution patterns at four weeks (**Figures S1B-S1E**). Furthermore, we observed greater multilineage potential of young HSCs, including lymphoid and myeloid reconstitution (LMPP/MPP4 and CLP, **Figures S1F and S1G**), when compared to old HSCs. Furthermore, young HSC recipients had significantly greater thymic cellularity and reconstitution of precursor and mature thymocytes than recipients of old HSCs (**Figures S1H-S1J**). In conclusion, old HSCs have significantly less multi-lineage potential, but especially T lymphoid potential than young HSCs in young allo-HCT recipients.

Age-related decline in multilineage HSCs marked by low Kit expression

Recent reports have shown remarkable functional heterogeneity of HSC[26, 27, 28, 29, 30, 31] subsets, highlighting discordance between current HSC phenotypic definitions to their molecular identities.[16, 17, 18] To identify HSCs with an enriched multilineage program and gain insights into their transcriptional and epigenetic framework, we performed multiome single-cell RNA and

ATAC sequencing on hematopoietic stem cells (LT-HSCs: Lineage$^-$CD34$^-$CD48$^-$CD150$^+$Sca-1$^+$c-Kit$^+$) from 2-mo (young) or 24-mo (old) female mice.

To define HSC subsets, we performed unsupervised Leiden cluster analysis on the multiome scRNA-seq data from our young cohort (**Figure S2A-S2B**). Using nomenclature and signatures derived from previous studies, [15, 16, 18, 32, 33, 34, 35] we mapped all unsupervised clusters into five main subsets (**Figure S2C**): Quiescent HSC (q-HSC), Platelet-biased HSC (Mgk-HSC), Multilineage HSC (MLin-HSC), Proliferative HSC (p-HSC), and a novel Intermediate HSC (Int-HSC) that showed overlapping features with Mgk-HSC, MLin-HSC and p-HSC subsets (**Data Table 1, Figure S2D**). To identify HSCs with multilineage potential, we compared multilineage enriched MLin-HSC versus low output q-HSC subsets in young HSCs and queried for previously described bonafide HSC markers (*Hlf, Kit, Neo1, Procr, CD244a, Pdzk1ip1, Ly9, Hoxb5*). *Hlf* and *Kit* had significantly higher expression in q-HSCs compared to MLin-HSCs (**Figure 1A**). *Hlf* has been previously implicated in HSC quiescence,[36, 37, 38] whereas *Kit* enriches for platelet-biased HSCs.[2] To further analyze the composition of HSCs with varying Kit expression, we defined Kit high and low HSC populations (Kit^{hi} and Kit^{lo} HSCs) based on the top and bottom 20% of *Kit* gene expression levels. We observed lower Kit expression in MLin-HSCs (**Figure 1B**) and increased representation of q-HSC and MLin-HSCs within the Kit^{lo} HSCs (**Figures 1C and S2E**), consistent with prior reports of increased self-renewal capacity and multipotency in Kit^{lo} HSCs.[1, 2]

To assess for age-associated changes, we first compared the transcriptional profile of young and old HSCs. In our differential gene analysis, we found that HSCs from young mice had higher expression of genes related to cell cycle (*Ccnd3, Cdc25a, Cdk1)*, and cell polarization (*Arhgap15*); conversely, old HSCs were enriched for expression of genes related to quiescence

(*Egr1*, *Junb*, *Jun*, *Jund*, *Fos*), platelet differentiation (*vWf*, *Clu*, *Itgb3*, *Fhl1 and Tgm2*), and myeloid differentiation (*Selp*, *Neo1*) (**Data Table 2**). Next to investigate age-related shifts in HSC cluster composition, we employed *ingest()* from scanpy to query the old HSC transcriptomic data using the "trained" young reference data for HSC subsets (**Figure S2F**). Subsequently, we generated a UMAP of our young and old datasets (**Figures S2G and 1D**) to visualize the post-ingestion results (**Figures 1E**). While all HSC subsets were present in young and old cohorts (**Figure 1F**), we notably observed an increased representation of MLin-HSCs, p-HSCs, and Int-HSCs in young HSCs. Conversely q-HSCs and Mgk-HSCs were predominantly in old HSCs (**Figures S2H- S2J**). Consistent with prior work,[18, 27, 39] these findings suggest shifts in the composition of HSC subsets with aging, indicating a reduction in multilineage potential accompanied by an increase in platelet bias.

Given the increased frequency of Mgk-HSCs in old HSCs and prior work[2] demonstrating that Kit^{hi} HSCs are platelet-biased HSCs (**Figures S2F- S2I**), we hypothesized this could be attributed to an expansion in Kit^{hi} HSCs. We observed significantly higher *Kit* expression (**Figures 1G-1H and S2K**) in old HSCs, with an age-dependent reduction in the proportion of Kit^{lo} HSCs accompanied by an increase in the frequency of Kit^{hi} HSCs (**Figure 1I**). Flow cytometry analysis of young and old bone marrow confirmed a significant expansion of Kit^{hi} HSCs, accompanied by a concomitant decrease in Kit^{lo} HSCs in old HSCs (**Figures S2L and 1J**), consistent with our prior report.[40] Together, these findings indicate that the frequency of multilineage Kit^{lo} HSCs declines with age.

Young Kit^{lo} HSCs exhibit enhanced T-cell potential

Next, we sought to determine the lymphoid potential of the HSC Kit subsets. To this end, we used the S17 lymphoid progenitor assay[41] to assess for lymphoid progenitor output of purified Kit^{hi} and Kit^{lo} HSCs from young mice (**Figure 2A**). Prior studies have elucidated the existence of functional heterogeneity among phenotypic Common Lymphoid Progenitors (CLPs) characterized by Ly6D expression,[42] resulting in the identification of two distinct subsets: All Lymphocyte Progenitors (ALPs), also referred to as functional CLPs, and B-cell biased Lymphocyte Progenitors (BLPs). Following 12-day co-culture, we observed that young Kit^{lo} HSCs generated more CLPs and ALPs than Kit^{hi} HSCs (**Figure 2B**). To further examine their T-cell differentiation potential, we used murine artificial thymic organoids (mATO, BM-ATO)[43, 44, 45] (**Figure 2A**). Following an 8-week culture, we noted a substantial increase in overall ATO output from young Kitl^{o} HSCs in comparison to Kit^{hi} HSCs (**Figure 2C**).

To further evaluate the reconstituting potential of Kit^{lo} HSCs, we competitively transplanted Kit^{lo} or Kit^{hi} HSCs from young C57BL/6 (CD45.2) mice with rescue BM cells (CD45.1) into lethally irradiated young BALB/cJ recipients (**Figure 2D**). Eight weeks after allo-HCT, we found that Kit^{lo} HSCs generated significantly better B- and T-cell reconstitution, while myeloid reconstitution was comparable (**Figures 2E, S3A-S3B**). Concordant with a prior report of better self-renewal ability,[2] we found that Kit^{lo} HSCs demonstrated increased LT HSC reconstitution (**Figure 2F**). In support of multilineage potential, we observed that Kit^{lo} HSC recipients had higher lymphoid progenitor reconstitution (including LMPP and CLP, **Figures 2F and 2G**), along with comparable myeloid precursor output (including MPP3, CMP, GMP, MEP, **Figures 2F and S3C**).

To evaluate whether enhanced lymphoid precursor output could contribute to thymic reconstitution, we concurrently evaluated the recipient thymi. We found that Kit^{lo} recipients

demonstrated enhanced thymic recovery, characterized by significantly higher thymic cellularity and reconstitution of precursor and mature thymocytes (**Figures 2H-2J**). Notably, in support of a critical role for thymocyte-stromal crosstalk in preserving thymic architecture,[11, 12, 13] we also found higher thymic epithelial cell (TEC), specifically medullary TEC, and endothelial cell recovery in Kit^{lo} reconstituted thymi (**Figures 2K and S3D**). We next examined donor-derived lymphoid progenitors for differential expression of molecules, involved in homing to the thymus (CCR7, CCR9, and PSGL1).[46] We observed significantly higher expression of CCR7 on Kit^{lo}-derived lymphoid progenitors (CLP) (**Figure S3E**). In addition, we analyzed thymic supernatants and found no differences in levels of thymopoietic ligands, IL22[47] and RANKL[48] (**Figure S3F**). Finally, we found significantly higher secondary lymphoid organ (spleen) reconstitution in Kit^{lo} recipients (**Figures S3G and S3H**). To evaluate long-term reconstitution, we performed additional harvests at 20-weeks following HCT. We observed similar trends in higher BM lymphopoiesis, thymic reconstitution, and thymic stromal recovery in Kit^{lo} recipients (**Figure S4**).

To assess thymic output, we used the RAG2-GFP model,[49] which allows the analysis of recent thymic emigrants (RTEs) (**Figure 2L**). We observed higher numbers of PB GFP+ T cells in Kit^{lo} recipients **(Figure 2M**). Additionally, to assess whether this increased number PB T cells in Kit^{lo} recipients results in increased functionality, (**Figure 2N**), we analyzed response to ovalbumin engineered *Listeria Monocytogenes* (LM-OVA) and observed a significant increase in OT1+ CD8+ T cells (**Figure 2O**).

A key element in the post-HCT recovery of thymic function is the influx of bone marrow-derived lymphoid progenitors, also known as thymic seeding progenitors (TSPs).[10] Furthermore, the significance of restoring the bone marrow-thymus axis in mitigating thymic involution has

been underscored through various strategies aimed at augmenting BM-lymphopoiesis, including sex-steroid ablation[50, 51] and administration of Ghrelin,[52] among other approaches.[53] We therefore hypothesized that robust BM lymphopoiesis driven by Kit^{lo} HSCs could potentially counteract age-related alterations within the thymic microenvironment, consequently ameliorating the decline in T-cell output. To this end, we competitively transplanted Kit^{lo} or Kit^{hi} HSCs from young C57BL/6 mice (CD45.2) with rescue BM cells (CD45.1) into lethally irradiated 14-month-old (Middle-aged) BALB/cJ recipients (**Figure 2P**). Sixteen weeks post-transplantation, we observed in Kit^{lo} vs Kit^{hi} recipients significantly higher numbers of peripheral T– and B-cells (**Figures 2Q, S3I, and S3J**). This was attributed to increased numbers of Kit^{lo} HSC-derived lymphoid progenitors (including LMPP/MPP4 and CLPs, **Figures S3K and S3L**), while numbers of myeloid precursors were comparable (MPP3, CMP, GMP, and MEP, **Figures S3K and S3M**). In our parallel analysis of the thymi of Kit^{lo} vs Kit^{hi} recipients, we observed increased numbers of thymocytes and TECs (**Figures 2R-2T and S3N**). Collectively, these findings establish the potential of Kit^{lo} HSCs for lymphopoiesis and to improve thymic recovery and peripheral T cell reconstitution in recipients of various ages.

Kit^{lo} HSCs exhibit distinct epigenetic features that facilitate lymphoid potential

Prior work has shown that immunophenotypically defined HSC clones with differential lymphoid output have distinct epigenetic signatures, with no discernable patterns in terms of gene expression.[18, 24, 54] To identify the gene regulatory network orchestrating the lymphoid potential differences in HSCs, we analyzed our single-cell ATAC-seq (scATAC-seq) component from our multiome dataset (**Figure S5D**). Through unsupervised clustering, we identified 6 clusters, including young and old HSCs (**Figures 3A and 3B**). Distinct HSC subsets identified

via scRNA-seq analyses (**Figure 1B**) are situated in varied regions on the scATAC-seq UMAP (**Figures 3C and 3D**). Notably, MLin-HSC and Kit^{lo} HSC intersect with Cluster 3 from the scATAC-seq clusters (**Figure 3E**).

We characterized the differentially accessible regions (DARs) of chromatin that defined the HSC subsets and found 2816 DARs in cluster C3 (MLin-HSC and Kit^{lo} enriched) cluster compared to cluster C6 (q-HSC and Kit^{hi} enriched) (**Figure S5F**). Next to determine the differential activity and accessibility of lymphoid-specifying transcription factors (TFs) in the identified Kit^{hi} and Kit^{lo} HSC subsets, we analyzed chromatin accessibility variation within TF motifs using chromVAR and gene accessibility. Compared to Kit^{hi} HSCs, we found increased gene accessibility and enrichment for Zinc finger motifs, specifically *Zbtb1 and Zbtb7a,* in Kit^{lo} DARs, which are implicated in lymphoid differentiation program[18, 55, 56, 57] (**Figures 3E-3F**).

In summary, we found that Kit^{lo} HSCs exhibit an epigenetic program, emphasizing an enrichment of lymphoid-specifying transcription factors, in support of their heightened lymphoid potential.

Zbtb1 **regulates T-cell potential in phenotypic HSCs**

Among members of the ZBTB gene family, *Zbtb1* plays a pivotal role in T-cell development[57, 58, 59] and lymphoid reconstitution.[57] However, its role in regulating lymphoid potential in HSCs remains unknown. We hypothesized that Zbtb1 loss impairs the lymphoid potential of Kit^{lo} HSCs. To this end, we used the CRISPR-Cas9 system to generate *Zbtb1*-deficient Kit^{lo} HSCs (**Figure 4A**) and confirmed decrease in Zbtb1 by flow-cytometric analysis (**Figure S6A**). *Zbtb1*-deficient Kit^{lo} HSCs showed significantly reduced *in vitro* T-cell potential (**Figure 4B**) and impaired lymphoid reconstitution *in vivo* (**Figure 4C**). Next, we questioned whether reinstating

Zbtb1 expression in megakaryocytic-biased, Kit^{hi} HSCs is sufficient to rescue their lymphoid defect. To test our hypothesis, we overexpressed *Zbtb1* cDNA in Kit^{hi} HSCs (**Figure 4D and S6B**) and we observed a rescue of their T-cell potential when compared to Kit^{hi} controls, thus partially phenocopying Kit^{lo} HSCs (**Figures 4E**) as well as improved lymphoid reconstitution *in vivo* (**Figure 4F**).

Previous studies have identified Zbtb1 targets which facilitate Notch-mediated T-cell differentiation in lymphoid progenitors[60] and support chromatin remodeling following DNA damage.[61] Given *Zbtb1* motif enrichment and enhanced T-cell differentiation in Kit^{lo} HSCs, we hypothesized that Zbtb1 targets mediating lymphoid differentiation gene programs are also enriched in Kit^{lo} HSCs. To this end, we queried Kit^{lo} enriched genes for Notch1-interacting proteins.[62] We observed ~50% overlap of Notch1-partners enriched in Kit^{lo} HSCs, of which 60% were Zbtb1-targets identified in a previous CHIP-seq study[60] (**Figure 4G**). Furthermore, we identified an additional subset of Zbtb1 targets (33%) that were not associated with the Notch1 interactome (**Data Table 3**). To further query for non-Notch related biological pathways, we performed pathway analysis and identified a strong enrichment for gene sets related to chromatin remodeling and RNA stability (**Figure 4H, Data Table 4**).

These data demonstrate that Zbtb1 contributes to an epigenetic regulatory program that facilitates T-cell differentiation in primitive Kit^{lo} HSCs likely through instructive and permissive mechanisms.

Old Kit^{lo} HSCs exhibit enhanced T-cell potential

To determine whether Kit^{lo} HSCs retain their lymphoid potential with age, we evaluated the lymphoid potential of old Kit subsets. Remarkably, even in the case of old mice, we noted a

substantial increase in lymphoid progenitor and ATO output from old Kit^{lo} HSCs compared to Kit^{hi} HSCs (**Figures 5A-5B**), although modest when compared to the young HSCs. This finding is consistent with prior reports of proliferative defects in aged T-cell precursors contributing to decreased thymopoiesis. [3, 4, 5]

Next, to test their *in vivo* potential, we competitively transplanted either Kit^{lo} or Kit^{hi} HSCs from old C57BL/6 (CD45.2) mice with rescue BM (CD45.1) cells into lethally irradiated young BALB/cJ recipients (**Figure 5C**). At eight weeks post-transplantation, we noted significantly higher numbers of T cells in the peripheral blood of Kit^{lo} vs Kit^{hi} recipients. (**Figures 5D and S7A**). Consistent with our experiments using HSCs from young donors, we observed in the BM of Kit^{lo} vs Kit^{hi} recipients significantly higher numbers of LT HSCs, LMPPs and CLPs (**Figures 5E-5F**) with comparable myeloid potential (**Figures 5E and S7B**). Furthermore, mirroring our findings in HSCs from young mice, we observed in recipients of old Kit^{lo} HSCs enhanced overall thymic cellularity, thymocyte reconstitution, and recovery of TECs and endothelial cells (**Figures 5G-5I and S7C-S7D**), increased CD4+ and CD8+ T cells in the spleen (**Figures S7E and S7F**), and higher RTE output (**Figures 5J-5K**). At 20-weeks post-HCT, we observed similar trends of enhanced reconstitution in old Kit^{lo} HSC recipients, confirming their long-term reconstituting potential (**Figure S7H-S7O**). Next to examine whether old HSC subsets with preserved lymphoid could augment aged thymic recovery, we competitively transplanted middle-aged recipients with old Kit^{lo} or Kit^{hi} donors (**Figure 5L**). We observed increased CLPs in the BM and peripheral T cells, but a modest, non-significant increase in thymic cellularity in Kit^{lo} recipients (**Figures 5M-5O, and S7G**). Similar to our *Zbtb1* functional studies with young Kit^{hi} HSCs, we observed a rescue in T-cell potential in *Zbtb1*-overexpressed old Kit^{hi} HSCs (**Figure 5P**).

Finally, to directly compare the per cell functionality of Kit^{lo} HSCs in the context of aging, we generated mixed chimeras combining Kit^{lo} HSCs cells from both young and old mice in an equal competition transplant (**Figure S8A**). Consistent with our *in vitro* findings (**Figures 5A-5B**), we found an overall decrease in lymphoid reconstitution within the PB, BM, and thymus with old Kit^{lo} HSCs when compared to their young counterparts (**Figures S8B-S8G**). Pathway analysis revealed decreased enrichment of chromatin remodeling related gene sets (**Figure S8H, Data Table 5**). Additionally, we noted decreased accessibility and expression of *Zbtb1 (***Figures S8I-S8K***)* in Old Kit^{lo} HSCs, indicating a impaired epigenetic program for lymphoid differentiation. These findings demonstrate that old Kit^{lo} HSCs exhibit preserved lymphoid potential and contribute to thymic recovery, albeit with reduced output.

KIT^{lo} human BM HSCs exhibit enhanced lymphoid potential

Informed by a recent study that mapped the molecular profiles of human thymic seeding progenitors (TSPs) to their transcriptional counterparts within the HSC compartment,[63] we next sought to identify a comparable human HSC subset with lymphoid potential. Interrogating a CITE-Seq dataset[64] generated from young and old human bone marrow (BM) samples (**Figures 6A-6C, S9A**), we mapped our mouse Kit^{lo} gene signature onto human HSCs and noted a significant enrichment in young BM (**Figures 6D and 6E**). We observed lower protein expression of KIT (CD117) on young HSCs by using antibody-derived tag (ADT) reads (**Figure S9B**). To validate our in-silico findings, we next assessed KIT expression in human BM samples (young: 20-40 years; middle-age/ old: >40 years). In our FACS analysis, we found that phenotypic HSCs (pHSCs: CD34+CD38-CD10-CD45RA-CD90+) showed the lowest KIT expression (**Figure S9C**), with higher KIT levels on old pHSCs (**Figure 6F**). Moreover, we

noted a statistically significant association between age and the composition of KIT subsets in pHSCs, indicating an increase in KIT^{hi} and a decrease in KIT^{lo} HSCs, aligning with our observations in mice. (**Figure 6G**).

Cord blood (CB) and BM have previously been fractionated based on KIT levels.[65, 66] To evaluate the T-cell potential of these human BM HSC subsets, we generated artificial human thymic organoids (huATOs) using purified KIT^{hi} or KIT^{lo} HSCs from human BM samples (**Figures S9D and 6H**; **Data Table 6**). In concordance with our mouse *in vitro* studies, following 8-10 weeks of culture, we observed significantly higher output of precursor and mature T-cells from KIT^{lo} HSCs- derived ATOs compared to KIT^{hi} HSCs (**Figure 6I**). To further evaluate the multilineage potential of KIT HSC subsets, we performed a lympho-myeloid differentiation assay, as previously described.[67] While we observed comparable myeloid differentiation potential, Kit^{lo} HSCs exhibited significantly more B cell and a non-significant increase in NK cell differentiation potential (**Figure 6J**).

Collectively, these results identify a previously uncharacterized subset of human BM HSCs, KIT^{lo} HSCs – which exhibit enhanced lymphoid potential.

DISCUSSION

Recent studies have uncovered significant heterogeneity within the HSC compartment and their role in hematopoiesis. This heterogeneity has implications for disease development and treatment. Of note, certain aspects of HSC heterogeneity challenge the established hematopoietic models, with lineage biases and lineage-restricted cells impacting self-renewal dynamics.[68, 69] Decisions regarding lympho-myeloid fate are established at multiple levels of the hematopoietic hierarchy: HSCs,[21, 22, 70] MPP, LMPP, and more mature GMPs and CLPs. At the level of HSCs,

the process of epigenetic imprinting confers a distinct advantage for lymphoid priming within multilineage HSCs, as well as maintaining these cell autonomous features imposed at steady state, even under conditions of stress.[18, 24]

Here, we report on the enhanced T-cell potential of Kit^{lo} HSCs, observed in both mice and humans. Through combining multiomic single-cell sequencing and functional analyses utilizing a preclinical allo-HCT model, we demonstrate augmented potential of Kit^{lo} HSCs for T-cell lymphopoiesis and to support thymic recovery, independent of age. During the early post-transplant period, we noted a relative increase in DN3 thymocytes relative to other thymocyte precursor subsets. This observation is consistent with previous studies reporting that DN3 thymocytes undergo compensatory expansion to support early post-transplant thymopoiesis, with minimal contribution from T-cell precursor thymocytes (ETP and DN2).[10, 71, 72] Further investigation into mechanisms driving these compensatory processes and its implications for immune function is critical to our understanding of post-transplant immune reconstitution.

Mechanistically, Kit^{lo} HSCs exhibit differential expression and activity of lymphoid-specifying transcription factors (TFs), including *Zbtb1*, indicating their epigenetic program towards a lymphoid fate. Studies in mouse models have shown that disruptions in *Zbtb1* result in T-cell developmental defects and severe combined immunodeficiency phenotypes,[57, 58] along with competitive disadvantages in B- and NK-cell compartments. [57] In our study, we identify *Zbtb1* as an essential transcription factor governing lymphoid specification in phenotypic HSCs and facilitating T-cell differentiation by reprogramming lineage biased Kit^{hi} HSCs. Additionally, we observed functional differences within Kit^{lo} HSCs in the context of aging, specifically a competitive disadvantage in Old Kit^{lo} HSCs, potentially attributable to their differences in

expression of the epigenetic repressor of multipotency, *Ezh1*,[73] and *Zbtb1*. Consistent with prior research, our study suggests *Zbtb1* modulates Notch-dependent[60] and cellular survival programs.[29, 74] However, further mechanistic studies are needed to elucidate the precise transcriptional mechanisms underlying this regulation. While the definitive role of *Zbtb1* in HSCs is not established, it may not have a direct role at the HSC stage; instead, its expression could be indicative of epigenetic states that facilitate or permit Zbtb1 expression and function at later stages of development, in lymphocyte progenitors. Future work will also address if ZBTB1 could be used to augment generation of mature lymphoid lineages from human BM precursors.

Long-term reconstituting CD34+KIT^{lo} human BM cells have been previously reported.[66] In contrast, fractionating phenotypic HSCs in Cord Blood (CB) based on KIT levels showed reduced reconstitution of KIT^{int} HSCs compared to KIT^{hi} HSCs.[65] These findings suggest that differences in Kit signaling have functional relevance depending on the developmental stage. In our study, combining transcriptional, immunophenotypic, and functional analyses of human BM samples we identified a KIT^{lo} subset within immunophenotypically defined HSCs with enhanced lymphoid potential, highlighting its translational relevance in human biology. Further functional characterization is warranted to definitively establish the clinical significance of thse observations. This understanding is crucial as prospective HSC isolation with subsequent ex vivo expansion,[75, 76] holds promise for enhancing immune regeneration after bone marrow transplantation, effectively counteracting treatment-related immunosuppression and age-associated thymic decline.

ACKNOWLEDGEMENTS

We thank Dr. Andrea Schietinger for the gift of mice; Ronan Chaligné, Kalina Belcheva, and Anthony Michaels for help; Dr. Gay Crooks, and Julia Gerscheimer (UCLA) for sharing the mATO and huATO systems and assistance with troubleshooting; Kenneth Dorshkind (UCLA) for providing S17 cells; Parashar Dhopala and Göran Karlsson (Lund University) for providing the human BM CITE-seq raw matrices.[64]

FUNDING SOURCES

This research was supported by National Cancer Institute award numbers, R35-CA284024, P01-CA023766, R01-CA228308, and P30 CA008748 MSK Cancer Center Support Grant/Core Grant; National Heart, Lung, and Blood Institute (NHLBI) award number R01-HL164902; National Institute on Aging award number P01-AG052359, and Tri Institutional Stem Cell Initiative. Additional funding was received from The Lymphoma Foundation, The Susan and Peter Solomon Family Fund, The Solomon Microbiome Nutrition and Cancer Program, Cycle for Survival, Parker Institute for Cancer Immunotherapy, Paula and Rodger Riney Multiple Myeloma Research Initiative, Starr Cancer Consortium, and Seres Therapeutics. HKE receives research support from NHLBI. SM receives research support from Marie-Josée Kravis fellowship in quantitative biology. SG receives research support from CRI / Donald J. Gogel Postdoctoral Fellowship (CRI #3934). SDW reports research funding from the MSK Leukemia SPORE Career Enhancement Program (NIH/NCI P50 CA254838-01), the MSK Gerstner Physician Scholar Program, and the Parker Institute for Cancer Immunotherapy. MS receives research support from the following funding sources: Burroughs Wellcome Fund (PDEP), Damon Runyon Cancer Research Foundation (Clinical Investigator Award), V Foundation (V Scholar), Emerson Collective, and the National Institutes of Health (NHLBI K08 HL156082-01A1). KA receives research support from the Gerstner Physician Scholar program.

AUTHOR CONTRIBUTIONS

HKE, MRMvdB conceived and designed the study. HKE, MRMvdB acquired funding. HKE, MBdS, AR, BG, NL, MAEA, SG planned research activities. HKE curated data and performed initial analysis. AIK and SM performed initial computational analysis of single-cell RNA- seq data, and single-cell ATAC- seq and human CITE-seq data, respectively. RS provided code and assisted HKE with downstream data/sequence computation and statistical analyses. HKE analyzed flow cytometric data. HKE, MBdS, AR, BG, NL, MAEA, XZ, HA, SG, MS, SDW, KV, CYP, CED, and JCS planned and performed experiments. CSL, AB, MRMvdB supervised study. HKE, SM, and MBdS prepared figures and visualized data. HKE, MRMvdB wrote the initial draft. All authors reviewed and approved the manuscript.

DECLARATION OF INTERESTS

H.K.Elias, and M.R.M. van den Brink are co-inventors on patent applications related to this work. MRMvdB has received research support and stock options from Seres Therapeutics and stock options from Notch Therapeutics and Pluto Therapeutics; he has received royalties from Wolters Kluwer; has consulted, received honorarium from or participated in advisory boards for Seres Therapeutics, WindMIL Therapeutics, Rheos Medicines, Merck & Co, Inc., Magenta Therapeutics, Frazier Healthcare Partners, Nektar Therapeutics, Notch Therapeutics, Forty Seven Inc., Priothera, Ceramedix, Lygenesis, Pluto Therapeutics, GlaskoSmithKline, Da Volterra, Vor BioPharma, Novartis (Spouse), Synthekine (Spouse), and Beigene (Spouse); he has IP Licensing with Seres Therapeutics and Juno Therapeutics; and holds a fiduciary role on the Foundation Board of DKMS (a nonprofit organization). The Walter and Eliza Hall Institute of Medical

Research receives milestone and royalty payments related to venetoclax. Employees are entitled to receive benefits related to these payments.

REFERENCES

1. Grinenko T, *et al.* Clonal expansion capacity defines two consecutive developmental stages of long-term hematopoietic stem cells. *J Exp Med* **211**, 209-215 (2014).

2. Shin JY, Hu W, Naramura M, Park CY. High c-Kit expression identifies hematopoietic stem cells with impaired self-renewal and megakaryocytic bias. *J Exp Med* **211**, 217-231 (2014).

3. Zediak VP, Maillard I, Bhandoola A. Multiple prethymic defects underlie age-related loss of T progenitor competence. *Blood* **110**, 1161-1167 (2007).

4. Min H, Montecino-Rodriguez E, Dorshkind K. Reduction in the developmental potential of intrathymic T cell progenitors with age. *J Immunol* **173**, 245-250 (2004).

5. Srinivasan J, *et al.* The initial age-associated decline in early T-cell progenitors reflects fewer pre-thymic progenitors and altered signals in the bone marrow and thymus microenvironments. *Aging Cell* **22**, e13870 (2023).

6. Hale JS, Boursalian TE, Turk GL, Fink PJ. Thymic output in aged mice. *Proc Natl Acad Sci U S A* **103**, 8447-8452 (2006).

7. van den Brink M, Uhrberg M, Jahn L, DiPersio JF, Pulsipher MA. Selected biological issues affecting relapse after stem cell transplantation: role of T-cell impairment, NK cells and intrinsic tumor resistance. *Bone Marrow Transplant* **53**, 949-959 (2018).

8. de Koning C, *et al.* CD4+ T-cell reconstitution predicts survival outcomes after acute graft-versus-host-disease: a dual-center validation. *Blood* **137**, 848-855 (2021).

9. van Roessel I, *et al.* Early CD4+ T cell reconstitution as predictor of outcomes after allogeneic hematopoietic cell transplantation. *Cytotherapy* **22**, 503-510 (2020).

10. Zlotoff DA, *et al.* Delivery of progenitors to the thymus limits T-lineage reconstitution after bone marrow transplantation. *Blood* **118**, 1962-1970 (2011).

11. van Ewijk W, Shores EW, Singer A. Crosstalk in the mouse thymus. *Immunol Today* **15**, 214-217 (1994).

12. Poliani PL, *et al.* Early defects in human T-cell development severely affect distribution and maturation of thymic stromal cells: possible implications for the pathophysiology of Omenn syndrome. *Blood* **114**, 105-108 (2009).

13. Pala F, *et al.* Profound abnormalities in thymic epithelial cells in Rag1 hypomorphic mice: implications for immune reconstitution after stem cell transplantation. *The Journal of Immunology* **208**, 167.102-167.102 (2022).

14. Elias HK, Bryder D, Park CY. Molecular mechanisms underlying lineage bias in aging hematopoiesis. *Semin Hematol* **54**, 4-11 (2017).

15. Rodriguez-Fraticelli AE, *et al.* Single-cell lineage tracing unveils a role for TCF15 in haematopoiesis. *Nature* **583**, 585-589 (2020).

16. Dong F, *et al.* Differentiation of transplanted haematopoietic stem cells tracked by single-cell transcriptomic analysis. *Nat Cell Biol* **22**, 630-639 (2020).

17. Carrelha J, *et al.* Hierarchically related lineage-restricted fates of multipotent haematopoietic stem cells. *Nature* **554**, 106-111 (2018).

18. Meng Y, *et al.* Epigenetic programming defines haematopoietic stem cell fate restriction. *Nat Cell Biol* **25**, 812-822 (2023).

19. Morita Y, Ema H, Nakauchi H. Heterogeneity and hierarchy within the most primitive hematopoietic stem cell compartment. *J Exp Med* **207**, 1173-1182 (2010).

20. Yamamoto R, *et al.* Large-Scale Clonal Analysis Resolves Aging of the Mouse Hematopoietic Stem Cell Compartment. *Cell Stem Cell* **22**, 600-607 e604 (2018).

21. Benz C, *et al.* Hematopoietic stem cell subtypes expand differentially during development and display distinct lymphopoietic programs. *Cell Stem Cell* **10**, 273-283 (2012).

22. Challen GA, Boles NC, Chambers SM, Goodell MA. Distinct hematopoietic stem cell subtypes are differentially regulated by TGF-beta1. *Cell Stem Cell* **6**, 265-278 (2010).

23. Naik SH, *et al.* Diverse and heritable lineage imprinting of early haematopoietic progenitors. *Nature* **496**, 229-232 (2013).

24. Yu VWC, *et al.* Epigenetic Memory Underlies Cell-Autonomous Heterogeneous Behavior of Hematopoietic Stem Cells. *Cell* **167**, 1310-1322 e1317 (2016).

25. Kondo M, Weissman IL, Akashi K. Identification of clonogenic common lymphoid progenitors in mouse bone marrow. *Cell* **91**, 661-672 (1997).

26. Flohr Svendsen A, *et al.* A comprehensive transcriptome signature of murine hematopoietic stem cell aging. *Blood* **138**, 439-451 (2021).

27. Grover A, *et al.* Single-cell RNA sequencing reveals molecular and functional platelet bias of aged haematopoietic stem cells. *Nat Commun* **7**, 11075 (2016).

28. Herault L, Poplineau M, Mazuel A, Platet N, Remy E, Duprez E. Single-cell RNA-seq reveals a concomitant delay in differentiation and cell cycle of aged hematopoietic stem cells. *BMC Biol* **19**, 19 (2021).

29. Kim YW, *et al.* Integration of single-cell transcriptomes and biological function reveals distinct behavioral patterns in bone marrow endothelium. *Nat Commun* **13**, 7235 (2022).

30. Konturek-Ciesla A, *et al.* Temporal multimodal single-cell profiling of native hematopoiesis illuminates altered differentiation trajectories with age. *Cell Rep* **42**, 112304 (2023).

31. Safi F, *et al.* Concurrent stem- and lineage-affiliated chromatin programs precede hematopoietic lineage restriction. *Cell Rep* **39**, 110798 (2022).

32. Giladi A, *et al.* Single-cell characterization of haematopoietic progenitors and their trajectories in homeostasis and perturbed haematopoiesis. *Nat Cell Biol* **20**, 836-846 (2018).

33. Cabezas-Wallscheid N, *et al.* Vitamin A-Retinoic Acid Signaling Regulates Hematopoietic Stem Cell Dormancy. *Cell* **169**, 807-823 e819 (2017).

34. Lauridsen FKB, *et al.* Differences in Cell Cycle Status Underlie Transcriptional Heterogeneity in the HSC Compartment. *Cell Rep* **24**, 766-780 (2018).

35. Cabezas-Wallscheid N, *et al.* Identification of regulatory networks in HSCs and their immediate progeny via integrated proteome, transcriptome, and DNA methylome analysis. *Cell Stem Cell* **15**, 507-522 (2014).

36. Wahlestedt M, *et al.* Critical Modulation of Hematopoietic Lineage Fate by Hepatic Leukemia Factor. *Cell Rep* **21**, 2251-2263 (2017).

37. Komorowska K, *et al.* Hepatic Leukemia Factor Maintains Quiescence of Hematopoietic Stem Cells and Protects the Stem Cell Pool during Regeneration. *Cell Rep* **21**, 3514-3523 (2017).

38. Lehnertz B, *et al.* HLF expression defines the human hematopoietic stem cell state. *Blood* **138**, 2642-2654 (2021).

39. Verovskaya E, *et al*. Heterogeneity of young and aged murine hematopoietic stem cells revealed by quantitative clonal analysis using cellular barcoding. *Blood* **122**, 523-532 (2013).

40. Elias HK, *et al.* Identification of Old HSCs with Preserved Self-Renewal and Long-Term Reconstitution Potential. *Blood* **134**, 2479 (2019).

41. Montecino-Rodriguez E, Kong Y, Casero D, Rouault A, Dorshkind K, Pioli PD. Lymphoid-Biased Hematopoietic Stem Cells Are Maintained with Age and Efficiently Generate Lymphoid Progeny. *Stem Cell Reports* **12**, 584-596 (2019).

42. Inlay MA, *et al.* Ly6d marks the earliest stage of B-cell specification and identifies the branchpoint between B-cell and T-cell development. *Genes Dev* **23**, 2376-2381 (2009).

43. Seet CS, *et al.* Generation of mature T cells from human hematopoietic stem and progenitor cells in artificial thymic organoids. *Nat Methods* **14**, 521-530 (2017).

44. Montel-Hagen A, *et al.* In Vitro Recapitulation of Murine Thymopoiesis from Single Hematopoietic Stem Cells. *Cell Rep* **33**, 108320 (2020).

45. Zhou W, Gao F, Romero-Wolf M, Jo S, Rothenberg EV. Single-cell deletion analyses show control of pro-T cell developmental speed and pathways by Tcf7, Spi1, Gata3, Bcl11a, Erg, and Bcl11b. *Sci Immunol* **7**, eabm1920 (2022).

46. Zlotoff DA, Sambandam A, Logan TD, Bell JJ, Schwarz BA, Bhandoola A. CCR7 and CCR9 together recruit hematopoietic progenitors to the adult thymus. *Blood* **115**, 1897-1905 (2010).

47. Dudakov JA, *et al.* Interleukin-22 drives endogenous thymic regeneration in mice. *Science* **336**, 91-95 (2012).

48. Lopes N, Vachon H, Marie J, Irla M. Administration of RANKL boosts thymic regeneration upon bone marrow transplantation. *EMBO Mol Med* **9**, 835-851 (2017).

49. Yu W, *et al.* Continued RAG expression in late stages of B cell development and no apparent re-induction after immunization. *Nature* **400**, 682-687 (1999).

50. Goldberg GL, *et al.* Sex steroid ablation enhances lymphoid recovery following autologous hematopoietic stem cell transplantation. *Transplantation* **80**, 1604-1613 (2005).

51. Goldberg GL, *et al.* Enhanced immune reconstitution by sex steroid ablation following allogeneic hemopoietic stem cell transplantation. *J Immunol* **178**, 7473-7484 (2007).

52. Dixit VD, *et al.* Ghrelin promotes thymopoiesis during aging. *J Clin Invest* **117**, 2778-2790 (2007).

53. Spadaro O, *et al.* Caloric restriction in humans reveals immunometabolic regulators of health span. *Science* **375**, 671-677 (2022).

54. Lara-Astiaso D, *et al.* Immunogenetics. Chromatin state dynamics during blood formation. *Science* **345**, 943-949 (2014).

55. Shin B, *et al.* Runx1 and Runx3 drive progenitor to T-lineage transcriptome conversion in mouse T cell commitment via dynamic genomic site switching. *Proc Natl Acad Sci U S A* **118**, (2021).

56. Maeda T, *et al.* Regulation of B versus T lymphoid lineage fate decision by the proto-oncogene LRF. *Science* **316**, 860-866 (2007).

57. Siggs OM, Li X, Xia Y, Beutler B. ZBTB1 is a determinant of lymphoid development. *J Exp Med* **209**, 19-27 (2012).

58. Punwani D, *et al.* Transcription factor zinc finger and BTB domain 1 is essential for lymphocyte development. *J Immunol* **189**, 1253-1264 (2012).

59. Zhang X, Lu Y, Cao X, Zhen T, Kovalovsky D. Zbtb1 prevents default myeloid differentiation of lymphoid-primed multipotent progenitors. *Oncotarget* **7**, 58768-58778 (2016).

60. Koizumi M, *et al.* Transcription factor Zbtb1 interacts with bridging factor Lmo2 and maintains the T-lineage differentiation capacity of lymphoid progenitor cells. *J Biol Chem* **298**, 102506 (2022).

61. Kim H, *et al.* Transcriptional repressor ZBTB1 promotes chromatin remodeling and translesion DNA synthesis. *Mol Cell* **54**, 107-118 (2014).

62. Yatim A, *et al.* NOTCH1 nuclear interactome reveals key regulators of its transcriptional activity and oncogenic function. *Mol Cell* **48**, 445-458 (2012).

63. Cordes M, *et al.* Single-cell immune profiling reveals thymus-seeding populations, T cell commitment, and multilineage development in the human thymus. *Sci Immunol* **7**, eade0182 (2022).

64. Sommarin MNE, *et al.* Single-Cell Multiomics Reveals Distinct Cell States at the Top of Human Hematopoietic Hierarchy. *bioRxiv*, 2021.2004.2001.437998 (2021).

65. Cosgun KN, *et al.* Kit regulates HSC engraftment across the human-mouse species barrier. *Cell Stem Cell* **15**, 227-238 (2014).

66. Kawashima I, Zanjani ED, Almaida-Porada G, Flake AW, Zeng H, Ogawa M. CD34+ human marrow cells that express low levels of Kit protein are enriched for long-term marrow-engrafting cells. *Blood* **87**, 4136-4142 (1996).

67. Karamitros D, *et al.* Single-cell analysis reveals the continuum of human lympho-myeloid progenitor cells. *Nat Immunol* **19**, 85-97 (2018).

68. Notta F, *et al.* Distinct routes of lineage development reshape the human blood hierarchy across ontogeny. *Science* **351**, aab2116 (2016).

69. Velten L, *et al.* Human haematopoietic stem cell lineage commitment is a continuous process. *Nat Cell Biol* **19**, 271-281 (2017).

70. Dykstra B, *et al.* Long-term propagation of distinct hematopoietic differentiation programs in vivo. *Cell Stem Cell* **1**, 218-229 (2007).

71. Paiva RA, *et al.* Self-renewal of double-negative 3 early thymocytes enables thymus autonomy but compromises the beta-selection checkpoint. *Cell Rep* **35**, 108967 (2021).

72. Maillard I, *et al.* Notch-dependent T-lineage commitment occurs at extrathymic sites following bone marrow transplantation. *Blood* **107**, 3511-3519 (2006).

73. Vo LT, *et al.* Regulation of embryonic haematopoietic multipotency by EZH1. *Nature* **553**, 506-510 (2018).

74. Cao X, Lu Y, Zhang X, Kovalovsky D. Zbtb1 Safeguards Genome Integrity and Prevents p53-Mediated Apoptosis in Proliferating Lymphoid Progenitors. *J Immunol* **197**, 1199-1211 (2016).

75. Sakurai M, *et al.* Chemically defined cytokine-free expansion of human haematopoietic stem cells. *Nature* **615**, 127-133 (2023).

76. Wilkinson AC, *et al.* Long-term ex vivo haematopoietic-stem-cell expansion allows nonconditioned transplantation. *Nature* **571**, 117-121 (2019).

77. Traag VA, Waltman L, van Eck NJ. From Louvain to Leiden: guaranteeing well-connected communities. *Sci Rep* **9**, 5233 (2019).

78. Wolock SL, Lopez R, Klein AM. Scrublet: Computational Identification of Cell Doublets in Single-Cell Transcriptomic Data. *Cell Syst* **8**, 281-291 e289 (2019).

79. Korsunsky I, *et al.* Fast, sensitive and accurate integration of single-cell data with Harmony. *Nat Methods* **16**, 1289-1296 (2019).

80. Kharchenko PV, Silberstein L, Scadden DT. Bayesian approach to single-cell differential expression analysis. *Nature methods* **11**, 740-742 (2014).

81. van Dijk D, *et al.* Recovering Gene Interactions from Single-Cell Data Using Data Diffusion. *Cell* **174**, 716-729 e727 (2018).

82. Finak G, *et al.* MAST: a flexible statistical framework for assessing transcriptional changes and characterizing heterogeneity in single-cell RNA sequencing data. *Genome Biol* **16**, 278 (2015).

83. Wolf FA, Angerer P, Theis FJ. SCANPY: large-scale single-cell gene expression data analysis. *Genome Biol* **19**, 15 (2018).

84. Dann E, Henderson NC, Teichmann SA, Morgan MD, Marioni JC. Differential abundance testing on single-cell data using k-nearest neighbor graphs. *Nat Biotechnol* **40**, 245-253 (2022).

85. Granja JM, *et al.* ArchR is a scalable software package for integrative single-cell chromatin accessibility analysis. *Nat Genet* **53**, 403-411 (2021).

86. Zhang Y, *et al.* Model-based analysis of ChIP-Seq (MACS). *Genome Biol* **9**, R137 (2008).

87. Schep AN, Wu B, Buenrostro JD, Greenleaf WJ. chromVAR: inferring transcription-factor-associated accessibility from single-cell epigenomic data. *Nat Methods* **14**, 975-978 (2017).

88. Hao Y, *et al.* Integrated analysis of multimodal single-cell data. *Cell* **184**, 3573-3587 e3529 (2021).

89. Cunningham F, *et al.* Ensembl 2022. *Nucleic Acids Res* **50**, D988-D995 (2022).

90. Johnson WE, Li C, Rabinovic A. Adjusting batch effects in microarray expression data using empirical Bayes methods. *Biostatistics* **8**, 118-127 (2007).

91. Fang Z, Liu X, Peltz G. GSEApy: a comprehensive package for performing gene set enrichment analysis in Python. *Bioinformatics* **39**, (2023).

FIGURE LEGENDS

Figure 1: Age-related decline in multilineage HSCs marked by low Kit expression

(**A-H**) Multiome single-cell RNA and ATAC sequencing was performed on HSC (Lineage-Sca-1+cKit+ CD34-CD48-Flt3-CD150+) cells isolated from 2-mo (young) or 24-mo (old) female C57BL/6 mice. nTOTAL =12,350 cells. (**A**) Volcano plot of DGE analysis between MLin-HSC vs. q-HSC subsets in young HSCs, highlighting bonafide HSC markers. (**B**) Violin plot for imputed *Kit* gene expression by annotated HSC subsets (as described in **Fig. S2C**. (**C**) Frequency of computationally defined HSC subtypes in Kit^{hi} and Kit^{lo} subsets in young HSCs. (**D-E**) Combined Uniform manifold approximation and projection (UMAP) of young and old HSCs after Harmony batch correction annotated by age **(D)** and annotated HSC subsets (q-HSC: Quiescent HSCs; Mgk-HSCs: Platelet-biased HSCs; Mlin-HSC: Multilineage HSCs; p-HSC: Proliferative HSCs; Int-HSC: Intermediate HSCs) **(E)**. **(F)** Frequency of HSC subtypes in young and old HSCs. **(G)** Heatmap showing gene expression of bonafide HSC markers ordered by increasing Kit expression. **(H)** Violin plot for imputed Kit gene expression by age. Statistical analysis was performed using the Wilcoxon test. **(I)** Scaled change in frequency for each Kit HSC subset with age. **(J)** FACS analysis showing frequency of Kit^{hi} and Kit^{lo} HSCs by age. All data are from n=6 mice/group. Error bars represent mean ± SEM. **P<0.01, ***P<0.001. P values calculated by two-way ANOVA.

Figure 2: Young Kit^{lo} HSCs exhibit enhanced T-cell potential

(A) Experimental schema to evaluate *in vitro* lymphoid progenitor and T-cell differentiation potential of Kit^{hi} (red) and Kit^{lo} HSCs (blue) from 2-mo (young) C57BL/6 mice using the S17 lymphoid assay and murine artificial thymic organoid (mATO) respectively. Enumeration of absolute number of lymphoid progenitor cells following 14 days in S17 lymphoid assay (B) and absolute number of T-cell subsets following 8-weeks of culture in mATOs **(C).** Aggregated data

across 4-5 independent experiments. **(D)** Experimental schema for competitive allogeneic HCT (allo-HCT) using Kit^{hi} (red) and Kit^{lo} HSCs (blue) from 2-mo (young) C57BL/6 mice with competitor bone marrow (BM) cells from B6.SJL-PtprcaPepcb/BoyJ mice transplanted into lethally irradiated 7-week-old (young) BALB/cJ recipients. **(E-K)** Eight weeks after competitive HCT, **(E)** frequency of donor-derived chimerism (CD45.2/ H-2Kb) of mature lineages in the peripheral blood (PB, CD45+, Myeloid cell: Gr1+CD11b+; B-cell: B220+; T-cell: CD3+), (**F-G)** Enumeration of absolute number of donor-derived cells in the BM for LSK cells (LT HSC: Lineage$^-$Sca-1$^+$cKit$^+$ CD34$^-$CD48$^-$Flt3$^-$CD150$^+$ **;** ST HSC: Lineage$^-$Sca-1$^+$cKit$^+$ CD48$^-$Flt3$^-$ CD150$^-$**;** MPP2: Lineage$^-$Sca-1$^+$cKit$^+$ CD48$^+$Flt3$^-$CD150$^-$; MPP3: Lineage$^-$Sca-1$^+$cKit$^+$ CD48$^+$Flt3$^-$CD150$^+$; MPP4/ LMPP: Lineage$^-$Sca-1$^+$cKit$^+$ Flt3$^+$CD150$^-$) **(F),** Common Lymphoid Progenitors cells (CLP: Lineage$^-$IL7Ra$^+$Flt3$^+$Sca$^{mid/lo}$ Kit^{lo}) **(G)**. **(H-K)** Post-HCT thymi analysis for total thymic cellularity **(H)**, **(I-J)** enumeration of absolute number of donor-derived cells for T-cell precursors (ETP: Lineage$^-$ CD4$^-$ CD8$^-$CD44$^+$ CD25$^-$Kit$^+$;DN2: Lineage$^-$ CD4$^-$ CD8$^-$CD44$^+$ CD25$^+$; DN3: Lineage$^-$ CD4$^-$ CD8$^-$CD44$^-$ CD25$^+$) **(I)**, Mature T-cells (DP: Lineage$^-$ CD4$^+$ CD8$^+$; SP4: Lineage$^-$ CD4$^+$ CD8$^-$; SP8: Lineage$^-$ CD4$^-$ CD8$^+$**)** **(J),** and analysis of thymic CD45- compartment for Thymic Epithelial Cells (TEC: CD45$^-$ EpCAM$^+$), Cortical TEC (cTEC: CD45$^-$ EpCAM$^+$UEA-1^{lo} 6C3^{hi} MHCII$^{hi/lo}$), and Medullary TEC (mTEC: CD45$^-$ EpCAM$^+$UEA-1^{hi} 6C3^{lo} MHCII$^{hi/lo-}$) (**K**). All data are from n=10-11 mice/group. **(L)** Experimental schema to evaluate thymic function following competitive allo-HCT using young HSCs. **(M)** Frequency of donor-derived Recent Thymic Emigrants (RTE: CD3+GFP+) in the PB at 8 weeks post-HCT. All data are from n=5-6 mice/group. **(N)** Experimental schema to investigate functional response of differential Kit-expressing HSC-derived T-cells in secondary recipients to *L. monocytogenes* expressing chicken ovalbumin (LM-OVA) infection. **(O)** Spleen analysis of secondary recipients

for frequency of OT1-derived chimerism of CD8+ T cells (OT1+CD8+: $Va2^{+}Vb5^{+}H2\text{-}K^{b}CD8^{+}$) 7 days post-infection. All data are from n=9-10 mice/group. **(P)** Experimental schema for competitive allogeneic HCT (allo-HCT) using Kit^{hi} (red) and Kit^{lo} HSCs (blue) from 2-mo (young) C57BL/6 mice with competitor bone marrow (BM) cells from B6.SJL-PtprcaPepcb/BoyJ mice transplanted into lethally irradiated 14-mo (Middle-aged) BALB/cJ recipients. **(Q)** Frequency of donor-derived T-cell chimerism at the indicated time-points. **(R-T)** Sixteen weeks after competitive HCT enumeration of total thymic cellularity **(R)**, donor-derived T-cell precursor thymocyte subsets as defined in Figure 3F **(S)**, donor-derived mature T-cell thymocyte subsets as defined in Figure 3G **(T).** All data are from n=6-7 mice/group. Error bars represent mean ± SEM. *P<0.05, **P<0.01, ***P<0.001, ****P<0.0001. P values calculated by nonparametric unpaired Mann-Whitney U test. Panels **A**, **D**, **L**, **N**, **and P** were created using BioRender.

Figure 3: Kit^{lo} HSCs exhibit distinct epigenetic features that facilitate lymphoid potential

(A) UMAP of 6 unsupervised HSC clusters identified by tile-based scATAC-seq analysis after Harmony batch correction. **(B-D)** Annotated by age **(B)**, HSC subsets **(C)**, and Kit subsets **(D)** on the scATAC-seq UMAP. **(E)** scATAC-seq cluster composition by HSC subsets (**left**) and Kit subsets (**right**). (**F-G**) Matrix plots showing motif enrichment identified by ChromVAR (**F**) and gene accessibility (**G**) for lymphoid-specifying transcription factors for Kit subsets in young and old HSCs.

Figure 4: *Zbtb1* regulates T-cell potential in phenotypic HSCs

(A) Experimental schema for T-cell differentiation assay and competitive allogeneic HCT with *Zbtb1*-deficient Kit^{lo} HSCs generated with 2-mo young Rosa26Cas9-eGFP KI mice. **(B)** Frequency of T-cell subsets following 6-weeks of culture in mATOs. Aggregated data across 3 independent experiments. (C) Frequency of donor-derived lineage chimerism of control or *Zbtb1* KO Kit^{lo} HSCs in the PB at 6 weeks following competitive HCT. All data are from n=5-6 mice/group. (D) Experimental schema for T-cell differentiation assay and competitive allogeneic HCT with *Zbtb1*-OE Kit^{hi} HSCs from young mice. (E) Frequency of T-cell subsets following 6-weeks of culture in mATO of young Kit^{hi} HSCs. Aggregated data across 3 independent experiments. (F) Frequency of donor-derived lineage chimerism of control or *Zbtb1* OE young Kit^{hi} HSCs in the PB at 6-weeks following competitive HCT. All data are from n=5-6 mice/group. (G) Previously identified Zbtb1-targets[60] and Notch1-interacting proteins[62] enriched in Kit^{lo} HSCs. (H) Pathway enrichment analysis for non-Notch1 Zbtb1-targets enriched in Kit^{lo} HSCs by *gseapy*()[91] using GO_Biological_Process_2023 libraries. Bubbleplot showing representative pathways. Error bars represent mean ± SEM. *P<0.05, **P<0.01, ***P<0.001. P values calculated by nonparametric unpaired Mann-Whitney U test. Panels **A** and **D** were created using BioRender.

Figure 5: Old Kit^{lo} HSCs exhibit enhanced T-cell potential

(A-B) Evaluation of *in vitro* lymphoid progenitor and T-cell differentiation potential of Kit^{hi} (red) and Kit^{lo} HSCs (blue) from or 24-mo (old) C57BL/6 mice using the S17 lymphoid assay and murine artificial thymic organoid (mATO) respectively, as shown in Figure 2A. Enumeration of absolute number of lymphoid progenitor cells following 14 days in S17 lymphoid assay **(A)** and absolute number of T-cell subsets following 8-weeks of culture in

mATOs **(B).** Aggregated data across 4-5 independent experiments. (**C)** Experimental schema for competitive allogeneic HCT (allo-HCT) using Kit^{hi} (red) and Kit^{lo} HSCs (blue) from 22–24-mo (old) C57BL/6 mice with competitor bone marrow (BM) cells from B6.SJL-PtprcaPepcb/BoyJ mice transplanted into lethally irradiated young BALB/cJ recipients. **(D-I)** Eight weeks after competitive HCT enumeration of absolute number of donor-derived T-cells in the PB **(D)**, LSK cell subsets as defined in Figure 3C (**E)**, CLP cells as defined in Figure 3D **(F)**, total thymic cellularity **(G)**, donor-derived T-cell precursor thymocyte subsets as defined in Figure 3F **(H)**, TEC compartment as defined in Figure 3H **(I).** All data are from n=9-10 mice/group. (**J)** Experimental schema to evaluate thymic function following competitive allo-HCT using old HSCs. **(K)** Frequency of donor-derived Recent Thymic Emigrants (RTE: CD3^{+}GFP^{+}) in the PB at 8 weeks post-HCT. All data are from n=5 mice/group. (**L)** Experimental schema for competitive allogeneic HCT (allo-HCT) using Kit^{hi} (red) and Kit^{lo} HSCs (blue) from 22-24-mo (old) C57BL/6 mice with competitor bone marrow (BM) cells from B6.SJL-PtprcaPepcb/BoyJ mice transplanted into lethally irradiated middle-aged BALB/cJ recipients. **(M-O)** Eight weeks after competitive HCT enumeration of absolute number of donor-derived T cells in PB **(M)**, donor-derived CLPs in the BM as defined in Figure 3D **(N)**, and thymic cellularity **(O)**. All data are from n=5-6 mice/group. (**P**) Frequency of T-cell subsets following 6-weeks of culture in mATO of old Kit^{hi} HSCs following *Zbtb1* OE. Aggregated data across 3 independent experiments. Error bars represent mean ± SEM. *P<0.05, **P<0.01, ***P<0.001, ****P<0.0001. P values calculated by nonparametric unpaired Mann-Whitney U test. Panels **C, J,** and **L** were created using BioRender.

Figure 6 KIT^{lo} human BM HSCs exhibit enhanced lymphoid potential

(A-E) Young and old human BM CITE-seq dataset generated and published by Sommarin et al.[64] **(A-C)** UMAP of CD34+ young and old human BM annotated with HSC subsets **(A)**, and age **(B)**. **(C)** HSC cluster composition by age. **(D)** Kit^{lo} gene signature (top 50 marker genes from our mouse data converted to human orthologues) was overlaid on human HSC UMAP. **(E)** Violin plot for Kit^{lo} gene score by age. Statistical analysis was performed using the Wilcoxon test. **(F-G)** FACS analysis of human BM samples. **(F)** Violin plot of KIT protein expression on phenotypic HSCs (pHSC: CD34+CD38-CD10-CD45RA-CD90+) by age (young: 20-40yrs; MA/old: >40yrs). **(G)** Scatterplot showing distribution of KIT^{hi} and KIT^{lo} HSC subsets within pHSCs in human BM samples with varying age. **(H)** Experimental schema to evaluate *in vitro* T-cell and lympho-myeloid potential of human BM HSC subsets based on differential KIT expression using human artificial thymic organoids (hATO) and MS5 assay respectively. **(I)** Following 8-10-weeks of culture, enumeration of CD19+ B-cells and T-cell subsets within CD34+ T-cell precursors (Early Thymic Progenitors, ETP: CD34^{+}CD1a^{-}CD7^{-} ; CD1a^{neg}- ProT: CD34^{+}CD1a^{-}CD7^{+}; CD1a^{pos}-ProT: CD34^{+}CD1a^{+}CD7^{+}), and mature T-cells (DP: CD34^{-}CD5^{+}CD7^{+}CD4^{+}CD8^{+}; SP4: CD34^{-}CD5^{+}CD7^{+}CD4^{+}CD8^{-} ; SP8: CD34^{-}CD5^{+}CD7^{+}CD4^{-}CD8^{+}). Aggregated data represent mean from 8 independent BM donors ± SEM. **(J)** Following 4-weeks of culture, enumeration of Lineage output (Neutrophil-Granulocytes: hCD45+CD15+; monocyte-macrophages: hCD45+CD14+; B-cells: hCD45+CD19+; NK-cells: hCD45+CD56+) after culturing 200 KIT^{lo} and KIT^{hi} HSC cells on MS-5 stroma, as previously described[67]. Aggregated data represent mean from 5 independent BM donors ± SEM. **(L)** Model illustrating age-related loss of lymphoid potential is attributed to a decreased in the frequency of Kit^{lo} HSCs in aged BM. Error bars represent mean ± SEM. *P<0.05, **P<0.01, ***P<0.001, ****P<0.0001. P values for panel **G** was based on generalized estimating equation logistic

model adjusted for age, KIT^{lo} and KIT^{hi} groups and their interaction, the matched data structure captured by an exchangeable working correlation structure. P values calculated either by nonparametric paired Mann-Whitney U test (Panels **I** and **J**), unpaired Mann-Whitney U test (Panel **F**). Panels **H** and **L** were created using BioRender.

Figure 1

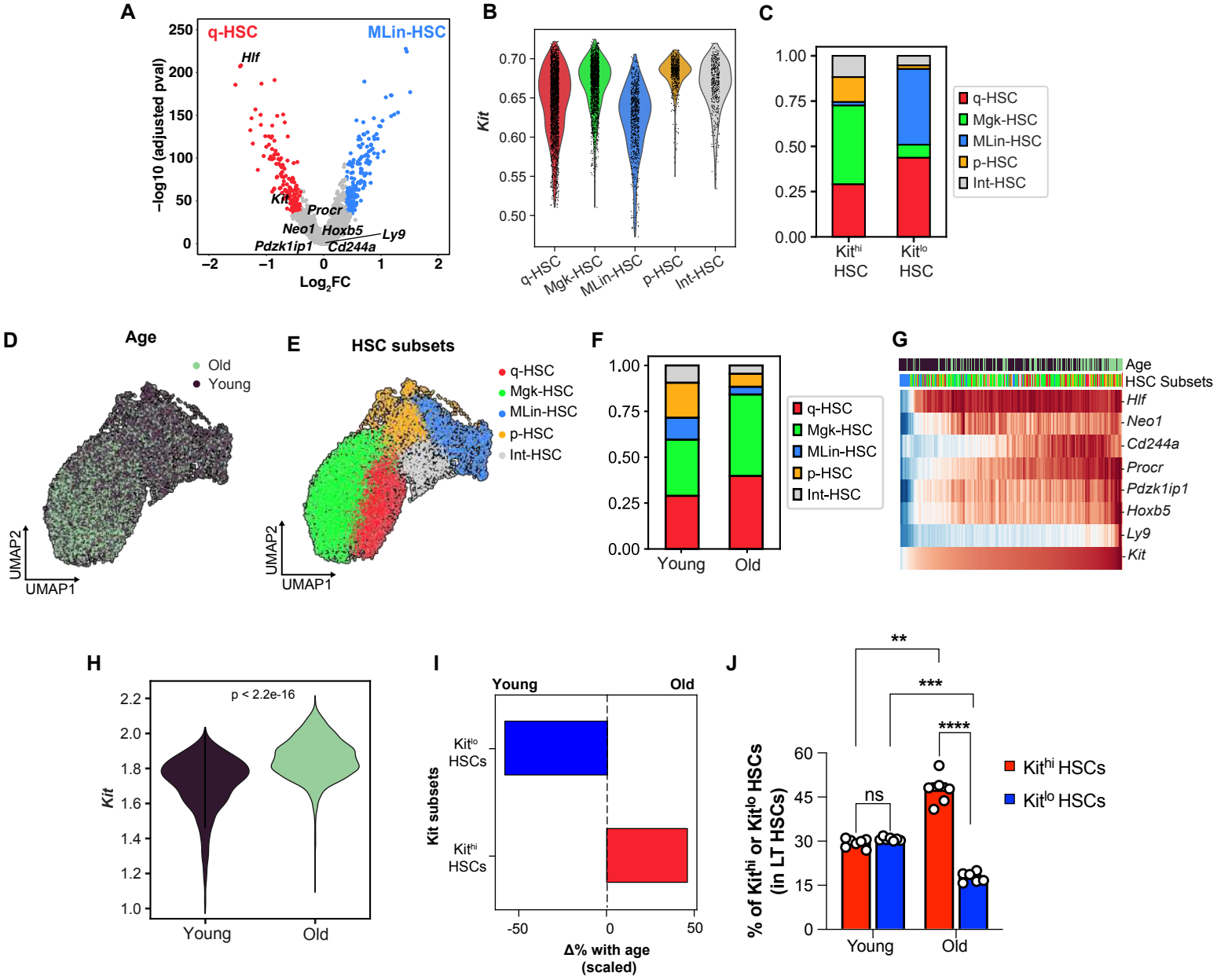
A
q-HSC
MLin-HSC
Hlf
Kit
Procr
Neo1
Hoxb5
Ly9
Pdzk1ip1
Cd244a
−log10 (adjusted pval)
Log2FC
B
Kit
q-HSC
Mgk-HSC
MLin-HSC
p-HSC
Int-HSC
C
Kithi HSC
Kitlo HSC
q-HSC
Mgk-HSC
MLin-HSC
p-HSC
Int-HSC
D
Age
Old
Young
UMAP2
UMAP1
E
HSC subsets
q-HSC
Mgk-HSC
MLin-HSC
p-HSC
Int-HSC
UMAP2
UMAP1
F
Young
Old
q-HSC
Mgk-HSC
MLin-HSC
p-HSC
Int-HSC
G
Age
HSC Subsets
Hlf
Neo1
Cd244a
Procr
Pdzk1ip1
Hoxb5
Ly9
Kit
H
p < 2.2e-16
Kit
Young
Old
I
Young
Old
Kit subsets
Kitlo HSCs
Kithi HSCs
Δ% with age (scaled)
J
**
***
****
ns
% of Kithi or Kitlo HSCs (in LT HSCs)
Kithi HSCs
Kitlo HSCs
Young
Old

Figure 2

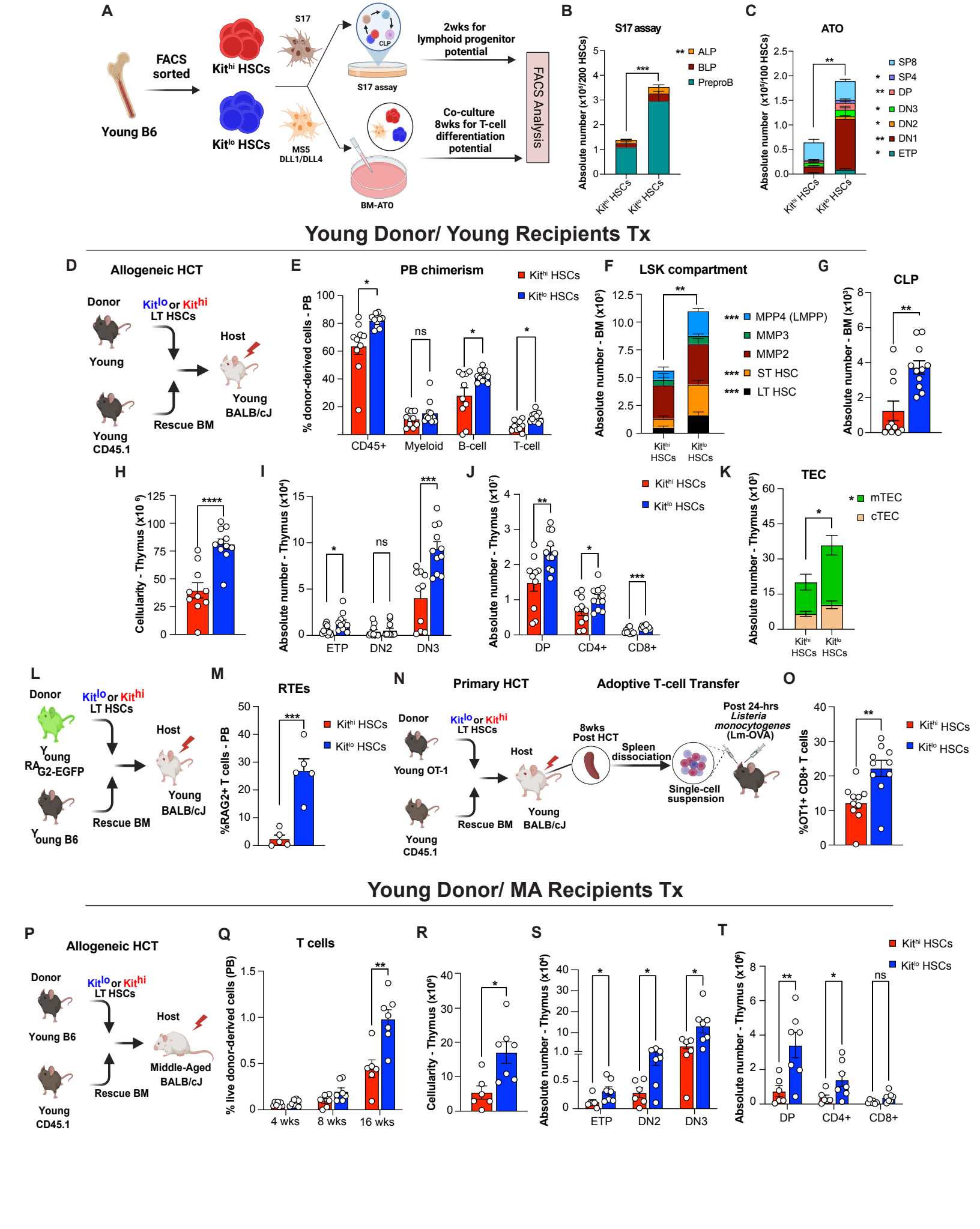
A
Young B6
FACS sorted
Kit^hi HSCs
Kit^lo HSCs
S17
MS5 DLL1/DLL4
CLP
S17 assay
BM-ATO
2wks for lymphoid progenitor potential
Co-culture 8wks for T-cell differentiation potential
FACS Analysis
B
S17 assay
Absolute number (x10^5/200 HSCs)
ALP
BLP
PreproB
C
ATO
Absolute number (x10^5/100 HSCs)
SP8
SP4
DP
DN3
DN2
DN1
ETP
Young Donor/ Young Recipients Tx
D
Allogeneic HCT
Donor
Kit^lo or Kit^hi LT HSCs
Young
Host
Young BALB/cJ
Rescue BM
Young CD45.1
E
PB chimerism
% donor-derived cells - PB
CD45+
Myeloid
B-cell
T-cell
F
LSK compartment
Absolute number - BM (x10^3)
MPP4 (LMPP)
MMP3
MMP2
ST HSC
LT HSC
G
CLP
Absolute number - BM (x10^3)
H
Cellularity - Thymus (x10^6)
I
Absolute number - Thymus (x10^4)
ETP
DN2
DN3
J
Absolute number - Thymus (x10^7)
DP
CD4+
CD8+
K
TEC
Absolute number - Thymus (x10^3)
mTEC
cTEC
L
Donor
Kit^lo or Kit^hi LT HSCs
Young RAG2-EGFP
Host
Young BALB/cJ
Rescue BM
Young B6
M
RTEs
%RAG2+ T cells - PB
N
Primary HCT
Adoptive T-cell Transfer
Donor
Kit^lo or Kit^hi LT HSCs
Young OT-1
Host
Young BALB/cJ
Rescue BM
Young CD45.1
8wks Post HCT
Spleen dissociation
Single-cell suspension
Post 24-hrs Listeria monocytogenes (Lm-OVA)
O
%OT1+ CD8+ T cells
Young Donor/ MA Recipients Tx
P
Allogeneic HCT
Donor
Kit^lo or Kit^hi LT HSCs
Young B6
Host
Middle-Aged BALB/cJ
Rescue BM
Young CD45.1
Q
T cells
% live donor-derived cells (PB)
4 wks
8 wks
16 wks
R
Cellularity - Thymus (x10^6)
S
Absolute number - Thymus (x10^4)
ETP
DN2
DN3
T
Absolute number - Thymus (x10^6)
DP
CD4+
CD8+

Figure 3

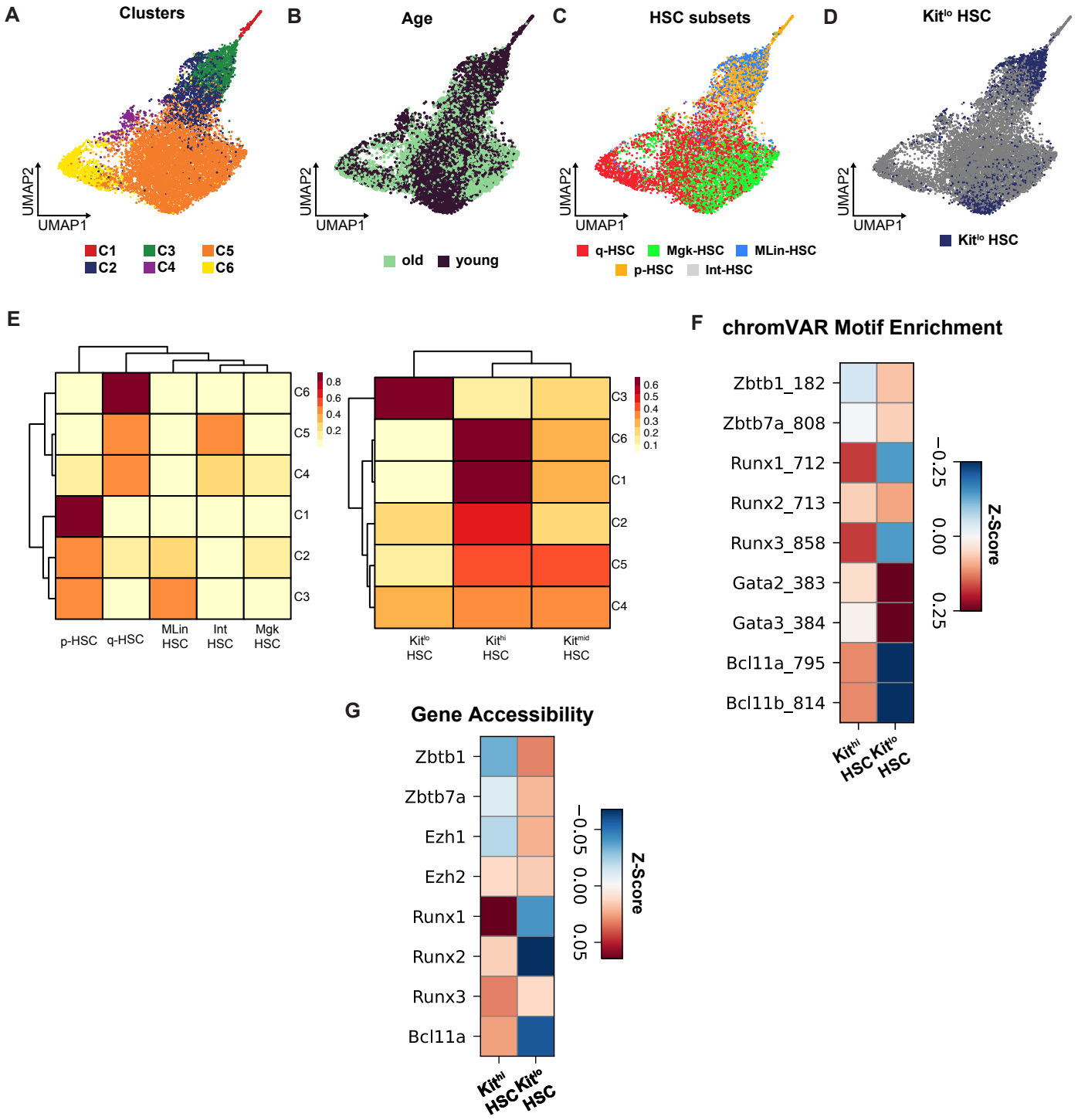
A
Clusters
UMAP2
UMAP1
C1
C2
C3
C4
C5
C6
B
Age
UMAP2
UMAP1
old
young
C
HSC subsets
UMAP2
UMAP1
q-HSC
Mgk-HSC
MLin-HSC
p-HSC
Int-HSC
D
Kit^{lo} HSC
UMAP2
UMAP1
Kit^{lo} HSC
E
C6
C5
C4
C1
C2
C3
p-HSC
q-HSC
MLin HSC
Int HSC
Mgk HSC
0.8
0.6
0.4
0.2
C3
C6
C1
C2
C5
C4
Kit^{lo} HSC
Kit^{hi} HSC
Kit^{mid} HSC
0.6
0.5
0.4
0.3
0.2
0.1
F
chromVAR Motif Enrichment
Zbtb1_182
Zbtb7a_808
Runx1_712
Runx2_713
Runx3_858
Gata2_383
Gata3_384
Bcl11a_795
Bcl11b_814
Kit^{hi} HSC
Kit^{lo} HSC
−0.25
0.00
0.25
Z-Score
G
Gene Accessibility
Zbtb1
Zbtb7a
Ezh1
Ezh2
Runx1
Runx2
Runx3
Bcl11a
Kit^{hi} HSC
Kit^{lo} HSC
−0.05
0.00
0.05
Z-Score

Figure 4

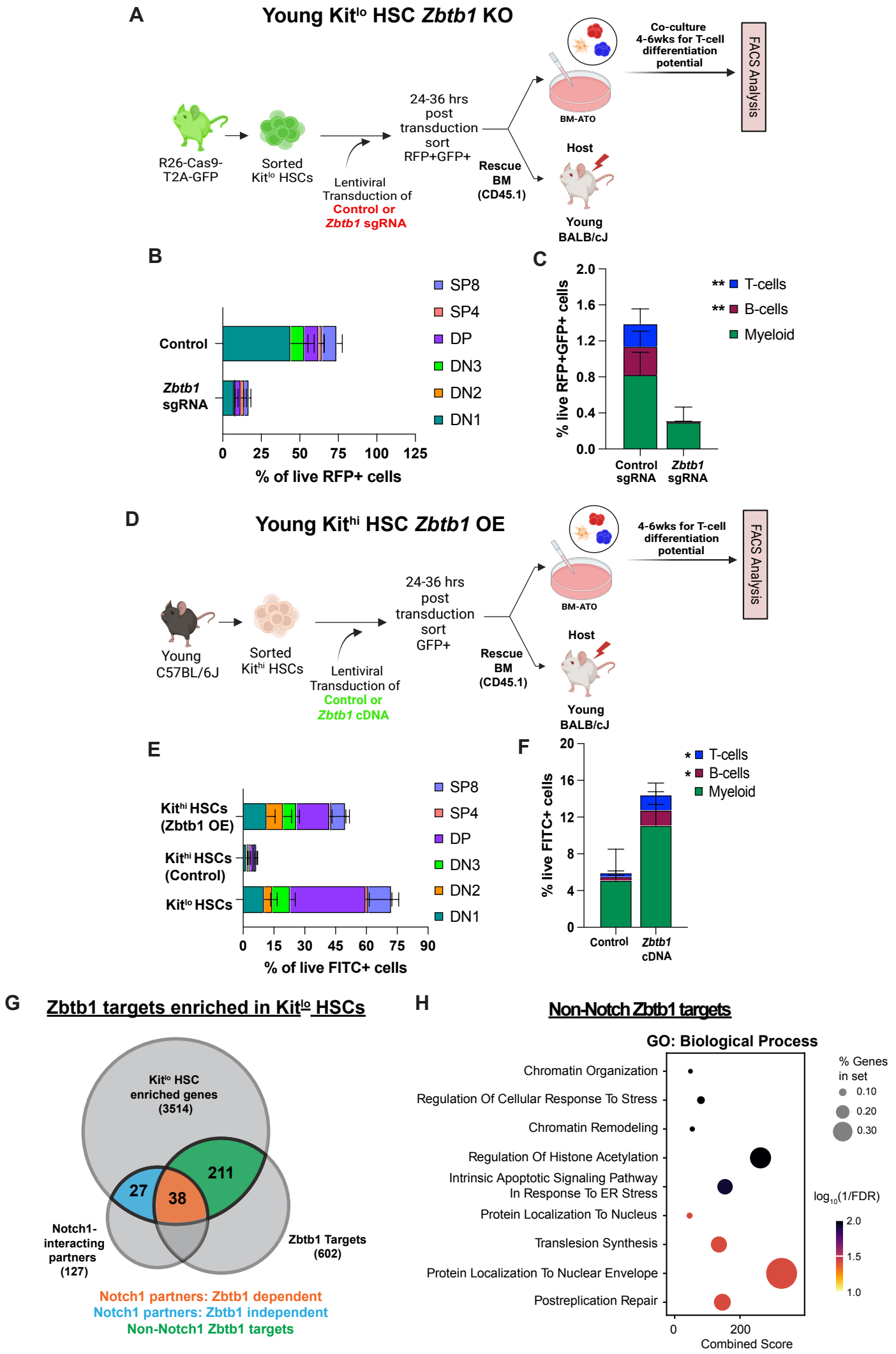
A
Young Kit^{lo} HSC Zbtb1 KO
R26-Cas9-T2A-GFP
Sorted Kit^{lo} HSCs
Lentiviral Transduction of Control or Zbtb1 sgRNA
24-36 hrs post transduction sort RFP+GFP+
Rescue BM (CD45.1)
BM-ATO
Co-culture 4-6wks for T-cell differentiation potential
FACS Analysis
Host
Young BALB/cJ
B
Control
Zbtb1 sgRNA
SP8
SP4
DP
DN3
DN2
DN1
0 25 50 75 100 125
% of live RFP+ cells
C
% live RFP+GFP+ cells
2.0 1.6 1.2 0.8 0.4 0.0
** T-cells
** B-cells
Myeloid
Control sgRNA
Zbtb1 sgRNA
D
Young Kit^{hi} HSC Zbtb1 OE
Young C57BL/6J
Sorted Kit^{hi} HSCs
Lentiviral Transduction of Control or Zbtb1 cDNA
24-36 hrs post transduction sort GFP+
Rescue BM (CD45.1)
BM-ATO
4-6wks for T-cell differentiation potential
FACS Analysis
Host
Young BALB/cJ
E
Kit^{hi} HSCs (Zbtb1 OE)
Kit^{hi} HSCs (Control)
Kit^{lo} HSCs
SP8
SP4
DP
DN3
DN2
DN1
0 15 30 45 60 75 90
% of live FITC+ cells
F
% live FITC+ cells
20 16 12 8 4 0
* T-cells
* B-cells
Myeloid
Control
Zbtb1 cDNA
G
Zbtb1 targets enriched in Kit^{lo} HSCs
Kit^{lo} HSC enriched genes (3514)
27
38
211
Notch1-interacting partners (127)
Zbtb1 Targets (602)
Notch1 partners: Zbtb1 dependent
Notch1 partners: Zbtb1 independent
Non-Notch1 Zbtb1 targets
H
Non-Notch Zbtb1 targets
GO: Biological Process
Chromatin Organization
Regulation Of Cellular Response To Stress
Chromatin Remodeling
Regulation Of Histone Acetylation
Intrinsic Apoptotic Signaling Pathway In Response To ER Stress
Protein Localization To Nucleus
Translesion Synthesis
Protein Localization To Nuclear Envelope
Postreplication Repair
0 200
Combined Score
% Genes in set
0.10
0.20
0.30
log$_{10}$(1/FDR)
2.0
1.5
1.0

Figure 5

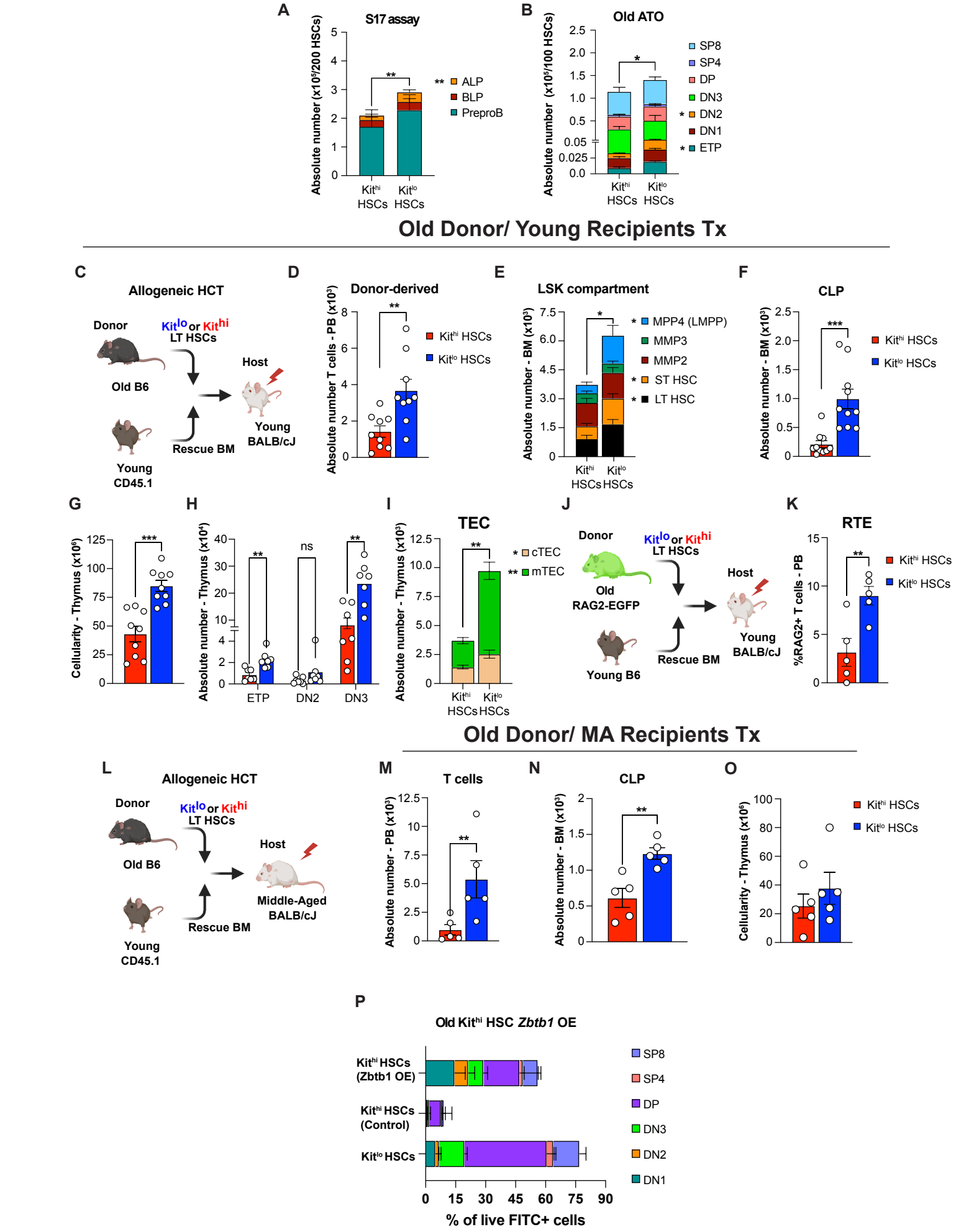
A
S17 assay
Absolute number (x10⁵/200 HSCs)
** ALP
BLP
PreproB
Kit^hi HSCs
Kit^lo HSCs
B
Old ATO
Absolute number (x10⁵/100 HSCs)
SP8
SP4
DP
DN3
* DN2
DN1
* ETP
Old Donor/ Young Recipients Tx
C
Allogeneic HCT
Donor
Kit^lo or Kit^hi LT HSCs
Old B6
Host
Young BALB/cJ
Rescue BM
Young CD45.1
D
Donor-derived
Absolute number T cells - PB (x10³)
Kit^hi HSCs
Kit^lo HSCs
E
LSK compartment
Absolute number - BM (x10³)
* MPP4 (LMPP)
MMP3
MMP2
* ST HSC
* LT HSC
F
CLP
Absolute number - BM (x10³)
G
Cellularity - Thymus (x10⁶)
H
Absolute number - Thymus (x10⁴)
ETP
DN2
DN3
ns
I
TEC
Absolute number - Thymus (x10³)
* cTEC
** mTEC
J
Donor
Old RAG2-EGFP
Young B6
Host
Young BALB/cJ
Rescue BM
K
RTE
%RAG2+ T cells - PB
Old Donor/ MA Recipients Tx
L
Allogeneic HCT
Donor
Old B6
Young CD45.1
Rescue BM
Middle-Aged BALB/cJ
M
T cells
Absolute number - PB (x10³)
N
CLP
Absolute number - BM (x10³)
O
Cellularity - Thymus (x10⁶)
P
Old Kit^hi HSC Zbtb1 OE
Kit^hi HSCs (Zbtb1 OE)
Kit^hi HSCs (Control)
Kit^lo HSCs
SP8
SP4
DP
DN3
DN2
DN1
% of live FITC+ cells

Figure 6

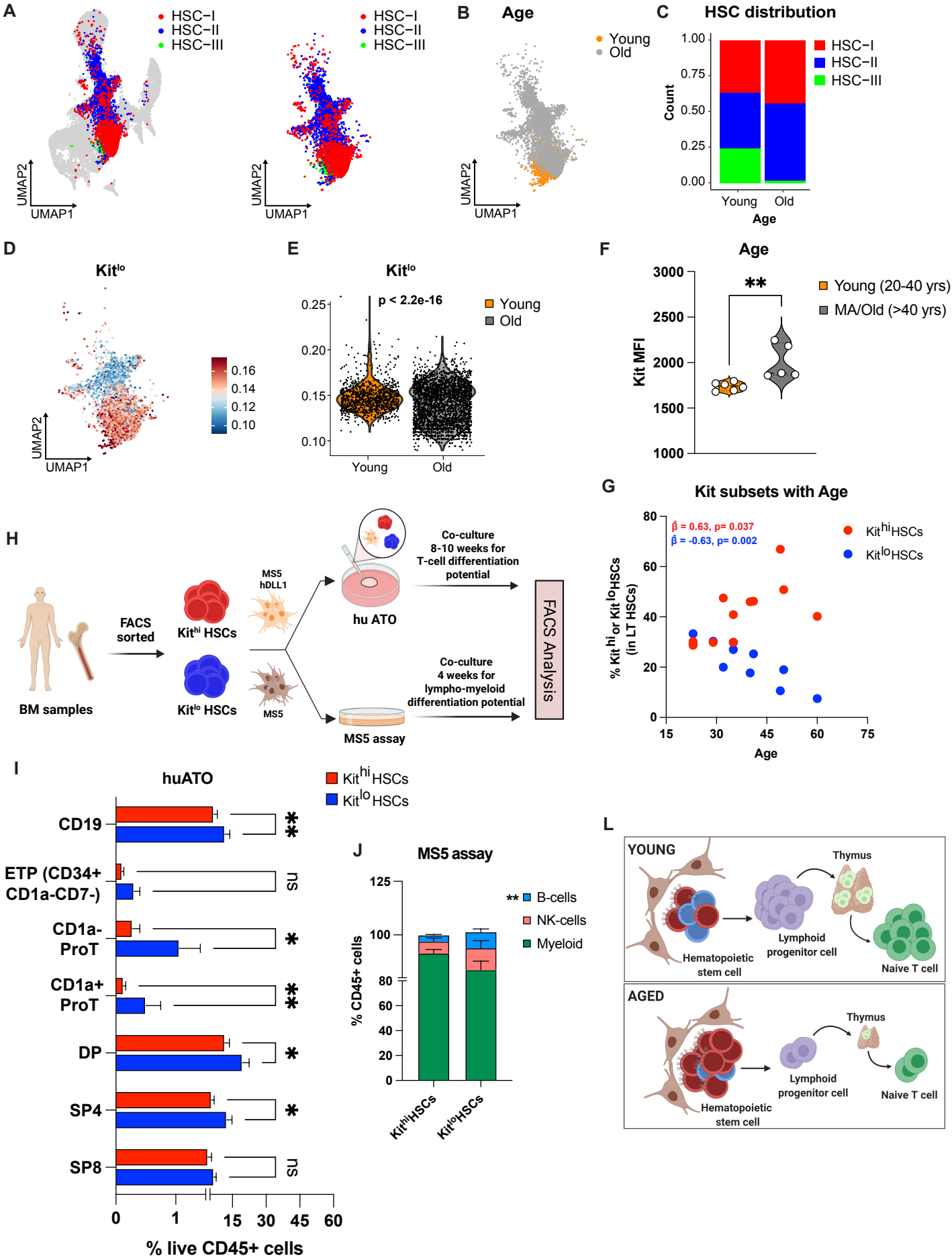
A
HSC−I
HSC−II
HSC−III
UMAP2
UMAP1
B
Age
Young
Old
C
HSC distribution
Count
Young
Old
Age
D
Kit^lo
0.16
0.14
0.12
0.10
E
Kit^lo
p < 2.2e-16
Young
Old
F
Age
Kit MFI
**
Young (20-40 yrs)
MA/Old (>40 yrs)
G
Kit subsets with Age
β̂ = 0.63, p= 0.037
β̂ = -0.63, p= 0.002
Kit^hi HSCs
Kit^lo HSCs
% Kit^hi or Kit^lo HSCs (in LT HSCs)
Age
H
BM samples
FACS sorted
Kit^hi HSCs
Kit^lo HSCs
MS5 hDLL1
MS5
hu ATO
MS5 assay
Co-culture 8-10 weeks for T-cell differentiation potential
Co-culture 4 weeks for lympho-myeloid differentiation potential
FACS Analysis
I
huATO
Kit^hi HSCs
Kit^lo HSCs
CD19
ETP (CD34+ CD1a-CD7-)
CD1a- ProT
CD1a+ ProT
DP
SP4
SP8
ns
% live CD45+ cells
J
MS5 assay
% CD45+ cells
B-cells
NK-cells
Myeloid
Kit^hi HSCs
Kit^lo HSCs
L
YOUNG
Thymus
Hematopoietic stem cell
Lymphoid progenitor cell
Naive T cell
AGED
Thymus
Hematopoietic stem cell
Lymphoid progenitor cell
Naive T cell

Figure S1

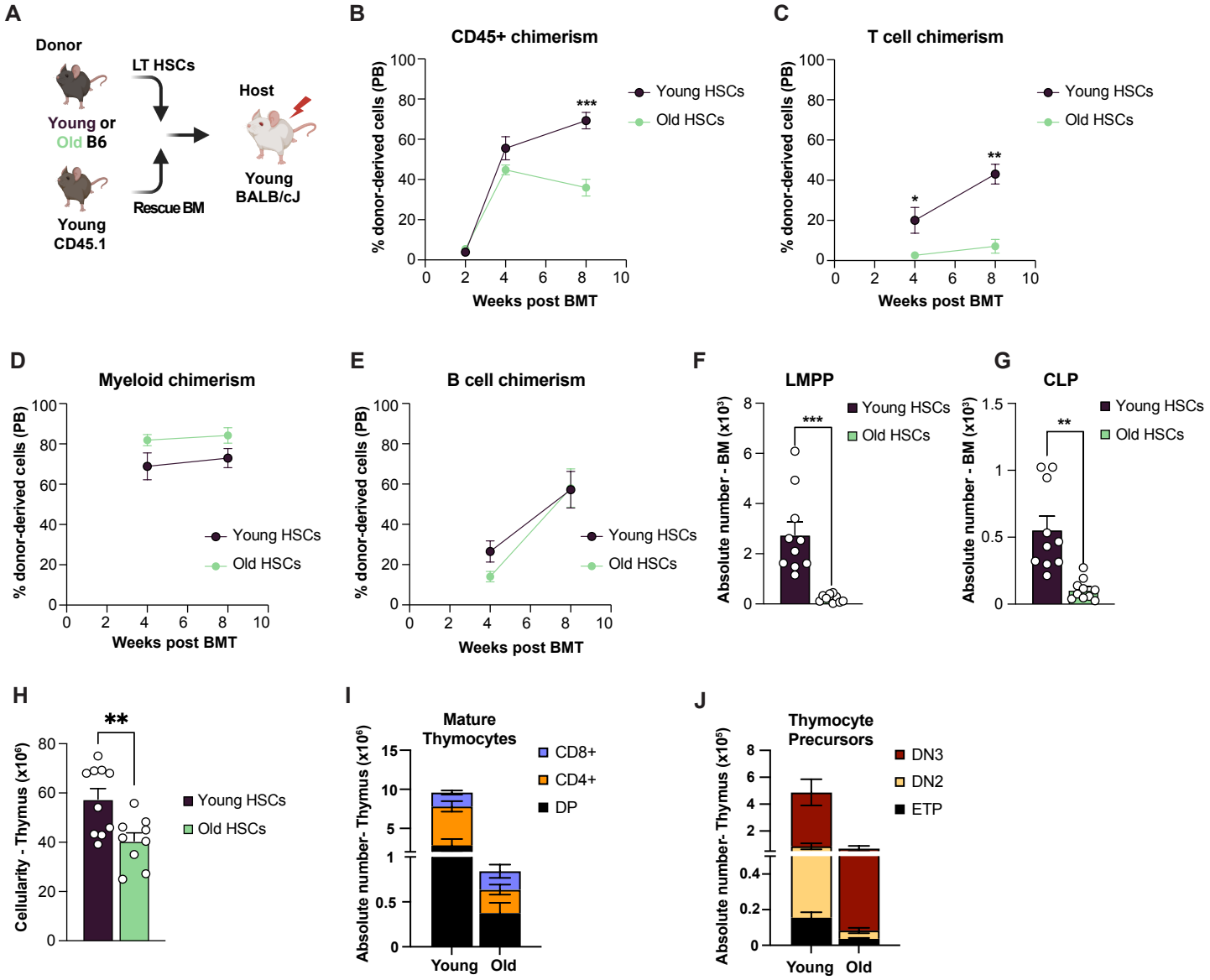
A
Donor
Young or
Old B6
Young
CD45.1
LT HSCs
Rescue BM
Host
Young
BALB/cJ
B
CD45+ chimerism
% donor-derived cells (PB)
Weeks post BMT
Young HSCs
Old HSCs
***
C
T cell chimerism
% donor-derived cells (PB)
Weeks post BMT
Young HSCs
Old HSCs
*
**
D
Myeloid chimerism
% donor-derived cells (PB)
Weeks post BMT
Young HSCs
Old HSCs
E
B cell chimerism
% donor-derived cells (PB)
Weeks post BMT
Young HSCs
Old HSCs
F
LMPP
Absolute number - BM (x10³)
Young HSCs
Old HSCs
***
G
CLP
Absolute number - BM (x10³)
Young HSCs
Old HSCs
**
H
Cellularity - Thymus (x10⁶)
Young HSCs
Old HSCs
**
I
Mature
Thymocytes
Absolute number- Thymus (x10⁶)
CD8+
CD4+
DP
Young
Old
J
Thymocyte
Precursors
Absolute number- Thymus (x10⁵)
DN3
DN2
ETP
Young
Old

Figure S2

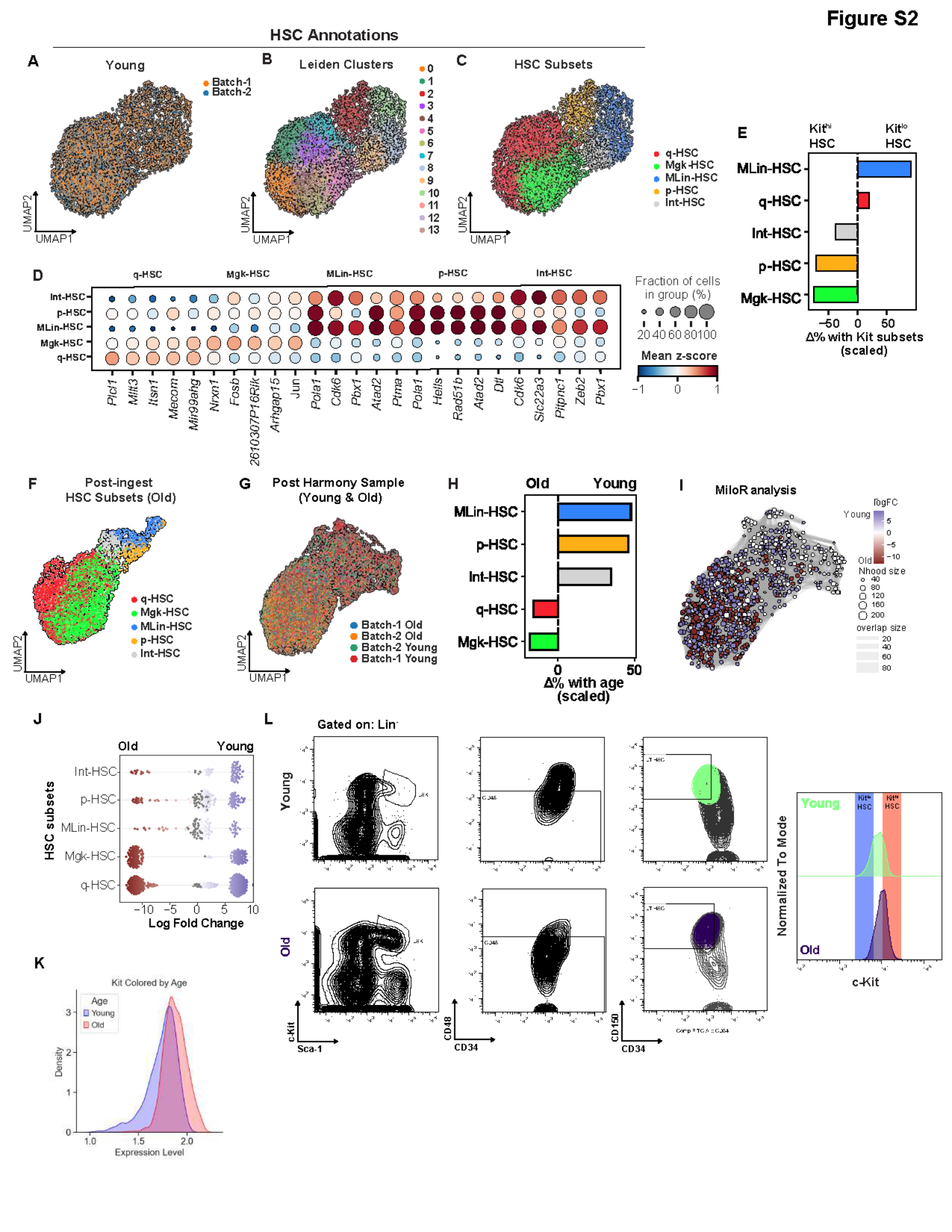
HSC Annotations
A
Young
Batch-1
Batch-2
UMAP2
UMAP1
B
Leiden Clusters
0
1
2
3
4
5
6
7
8
9
10
11
12
13
C
HSC Subsets
q-HSC
Mgk-HSC
MLin-HSC
p-HSC
Int-HSC
D
q-HSC
Mgk-HSC
MLin-HSC
p-HSC
Int-HSC
Plcl1
Mllt3
Itsn1
Mecom
Mir99ahg
Nrxn1
Fosb
2610307P16Rik
Arhgap15
Jun
Pola1
Cdk6
Pbx1
Atad2
Ptma
Pola1
Hells
Rad51b
Atad2
Dtl
Cdk6
Slc22a3
Plpnc1
Zeb2
Pbx1
Fraction of cells in group (%)
20 40 60 80 100
Mean z-score
−1
0
1
E
Kit^hi HSC
Kit^lo HSC
MLin-HSC
q-HSC
Int-HSC
p-HSC
Mgk-HSC
−50
0
50
Δ% with Kit subsets (scaled)
F
Post-ingest HSC Subsets (Old)
q-HSC
Mgk-HSC
MLin-HSC
p-HSC
Int-HSC
UMAP2
UMAP1
G
Post Harmony Sample (Young & Old)
Batch-1 Old
Batch-2 Old
Batch-2 Young
Batch-1 Young
UMAP2
UMAP1
H
Old
Young
MLin-HSC
p-HSC
Int-HSC
q-HSC
Mgk-HSC
0
50
Δ% with age (scaled)
I
MiloR analysis
logFC
Young
5
0
−5
−10
Old
Nhood size
40
80
120
160
200
overlap size
20
40
60
80
J
Old
Young
HSC subsets
Int-HSC
p-HSC
MLin-HSC
Mgk-HSC
q-HSC
−10
−5
0
5
10
Log Fold Change
K
Kit Colored by Age
Age
Young
Old
Density
0
1
2
3
1.0
1.5
2.0
Expression Level
L
Gated on: Lin⁻
Young
Old
c-Kit
Sca-1
CD48
CD34
CD150
CD34
Young
Old
Kit^lo HSC
Kit^hi HSC
Normalized To Mode
c-Kit

Figure S3

Young Donor/ Young Recipients Tx

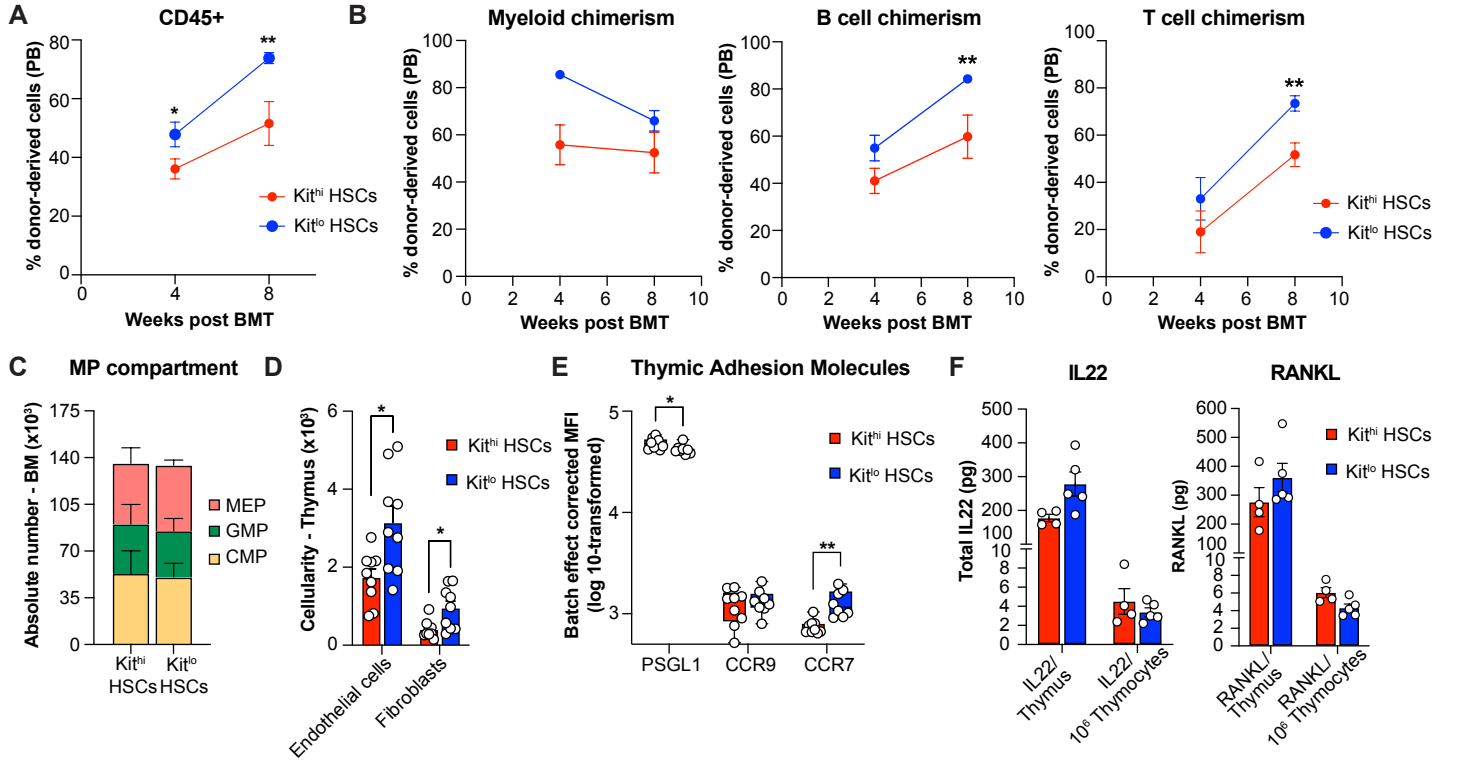

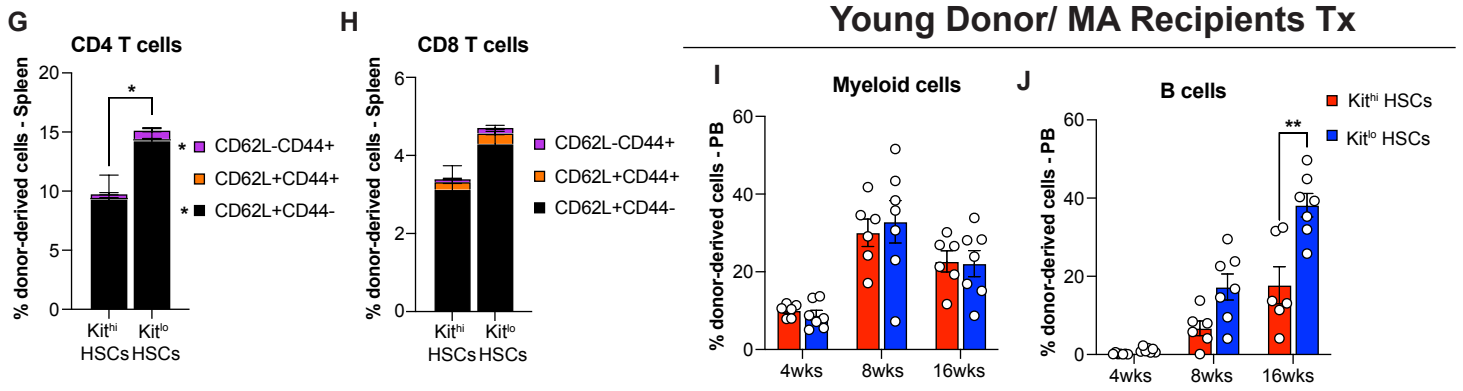

Young Donor/ MA Recipients Tx

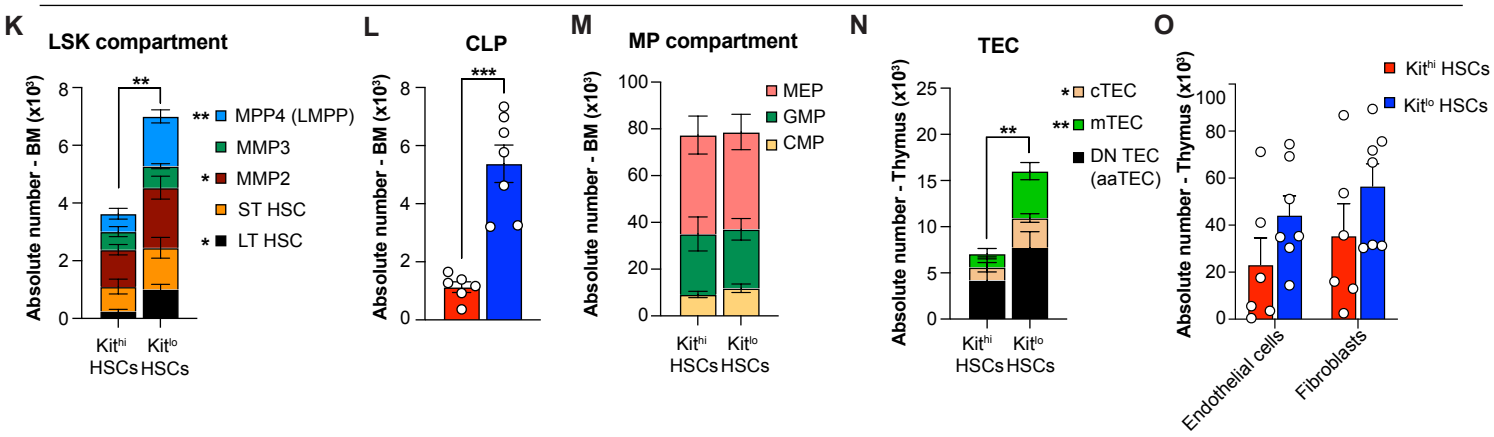

Young 20-week Post HCT

Figure S4

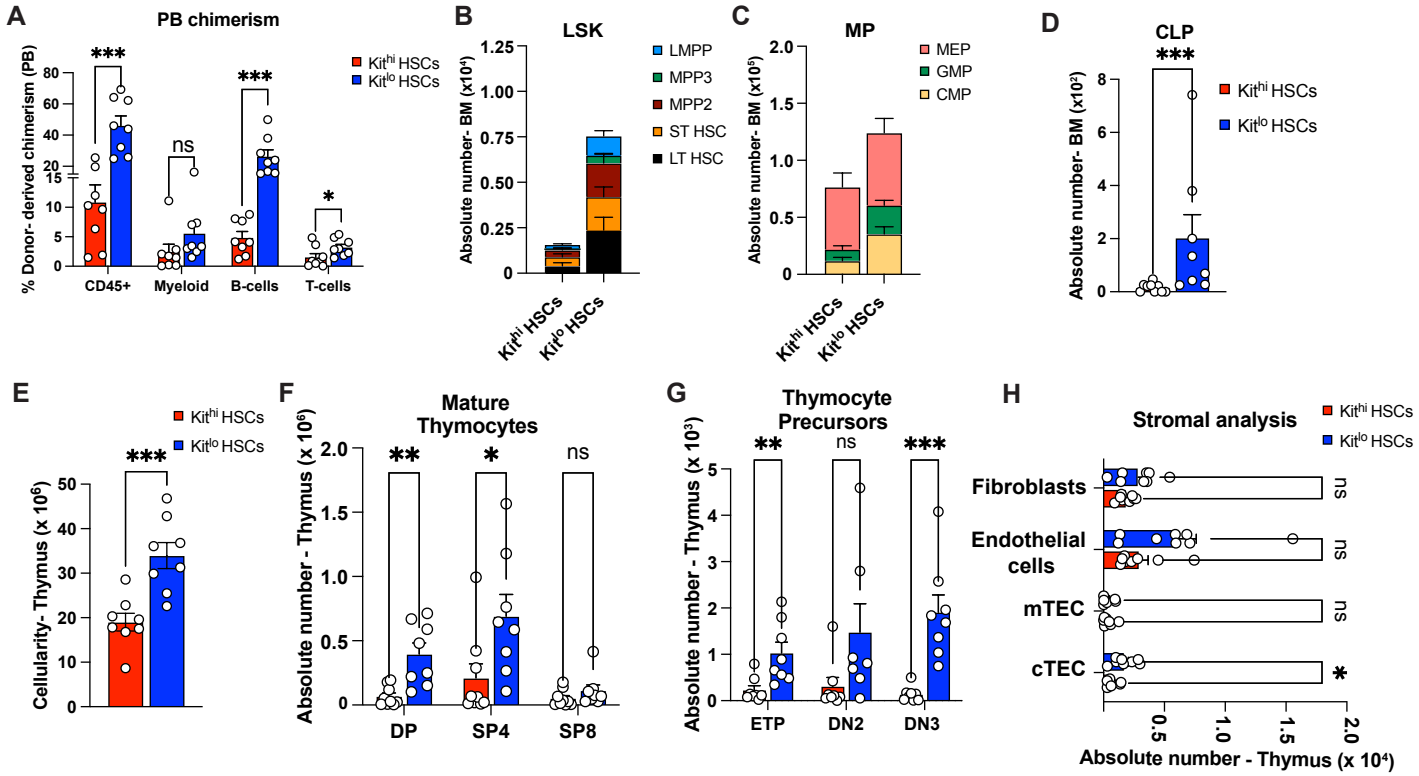

Figure S5

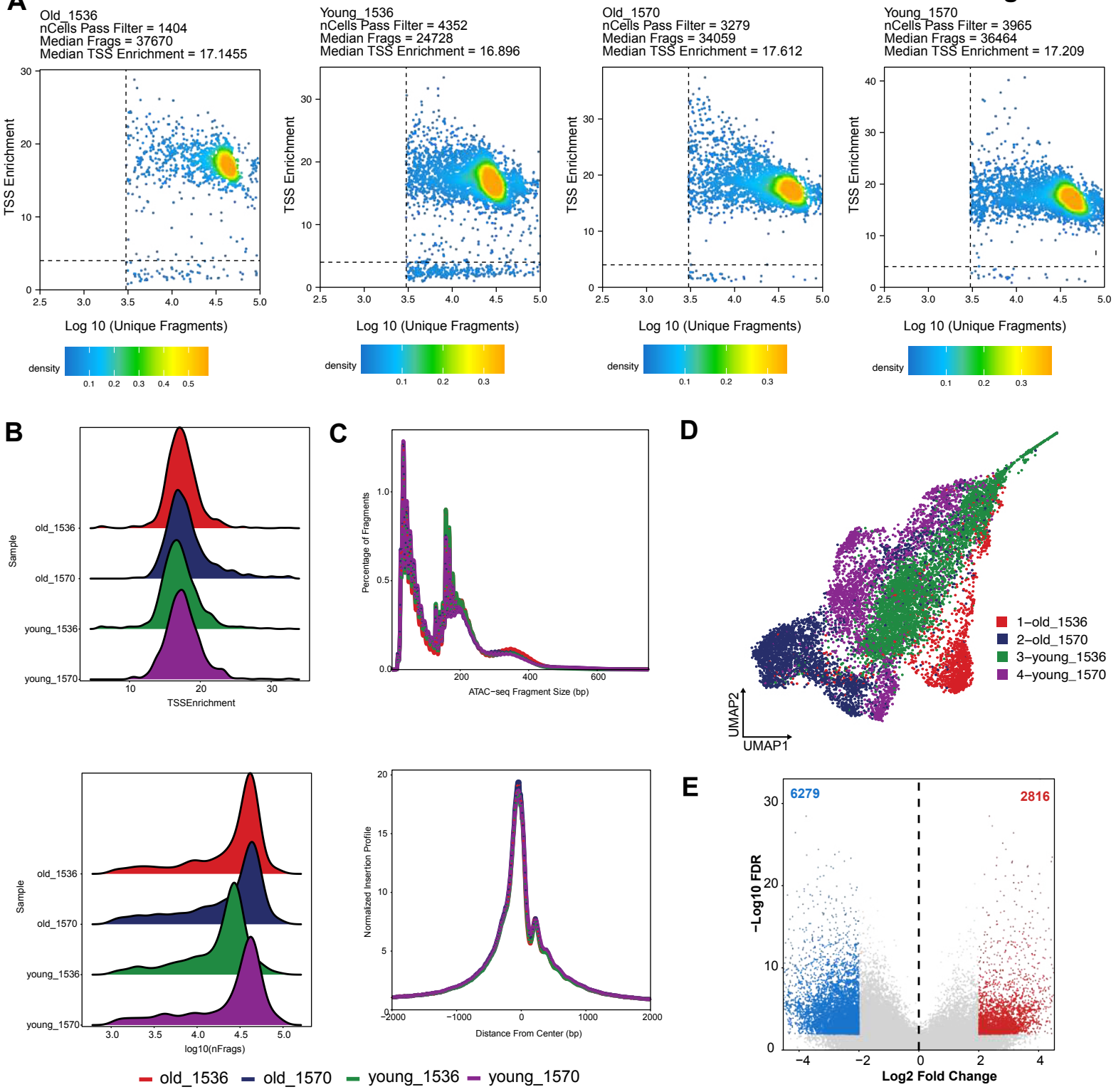
A
Old_1536
nCells Pass Filter = 1404
Median Frags = 37670
Median TSS Enrichment = 17.1455
Young_1536
nCells Pass Filter = 4352
Median Frags = 24728
Median TSS Enrichment = 16.896
Old_1570
nCells Pass Filter = 3279
Median Frags = 34059
Median TSS Enrichment = 17.612
Young_1570
nCells Pass Filter = 3965
Median Frags = 36464
Median TSS Enrichment = 17.209
TSS Enrichment
Log 10 (Unique Fragments)
density
B
Sample
old_1536
old_1570
young_1536
young_1570
TSSEnrichment
C
Percentage of Fragments
ATAC−seq Fragment Size (bp)
D
UMAP2
UMAP1
1−old_1536
2−old_1570
3−young_1536
4−young_1570
log10(nFrags)
Normalized Insertion Profile
Distance From Center (bp)
E
6279
2816
−Log10 FDR
Log2 Fold Change
old_1536
old_1570
young_1536
young_1570

Figure S6

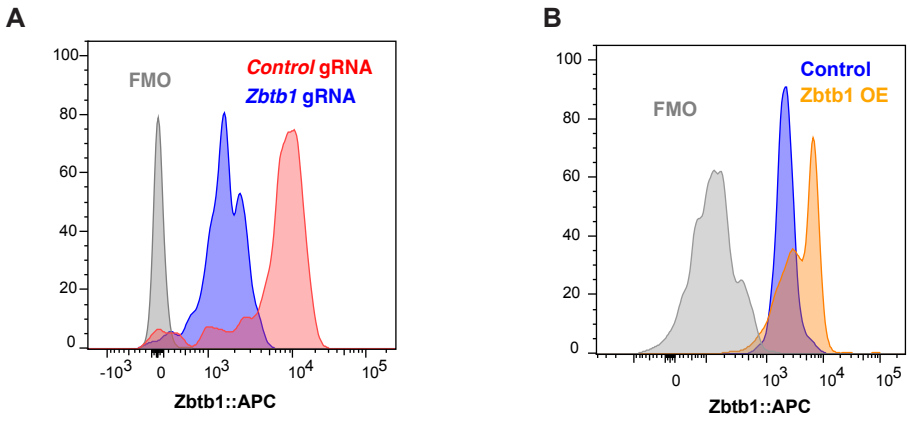
A
FMO
Control gRNA
Zbtb1 gRNA
100
80
60
40
20
0
-10^3
0
10^3
10^4
10^5
Zbtb1::APC
B
FMO
Control
Zbtb1 OE
100
80
60
40
20
0
0
10^3
10^4
10^5
Zbtb1::APC

Figure S7

Old Donor/ Young Recipients Tx

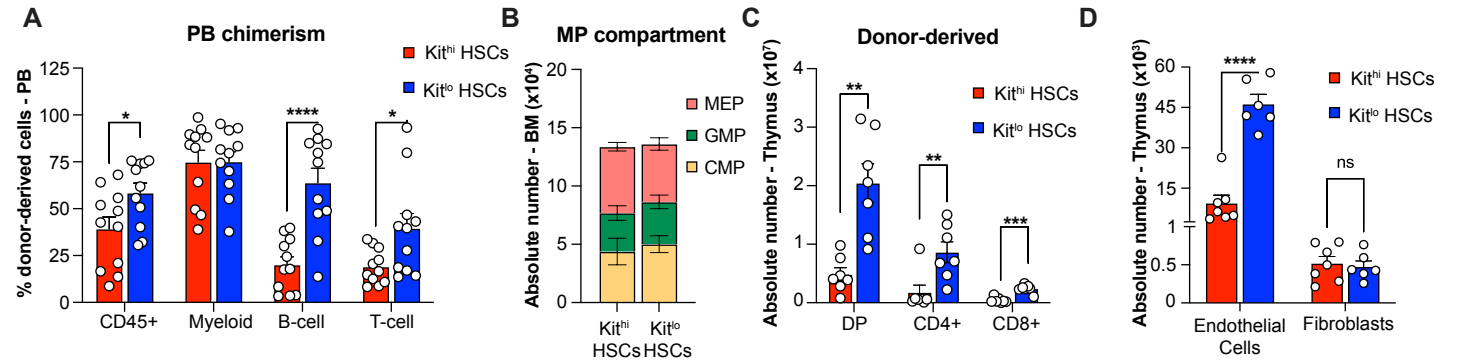

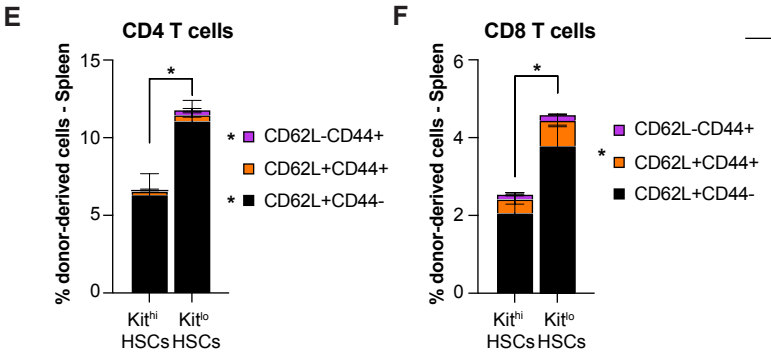

Old Donor/ MA Recipients Tx

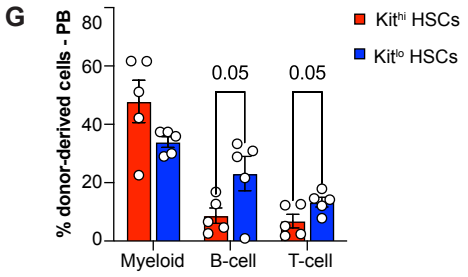

Old 20-week Post HCT

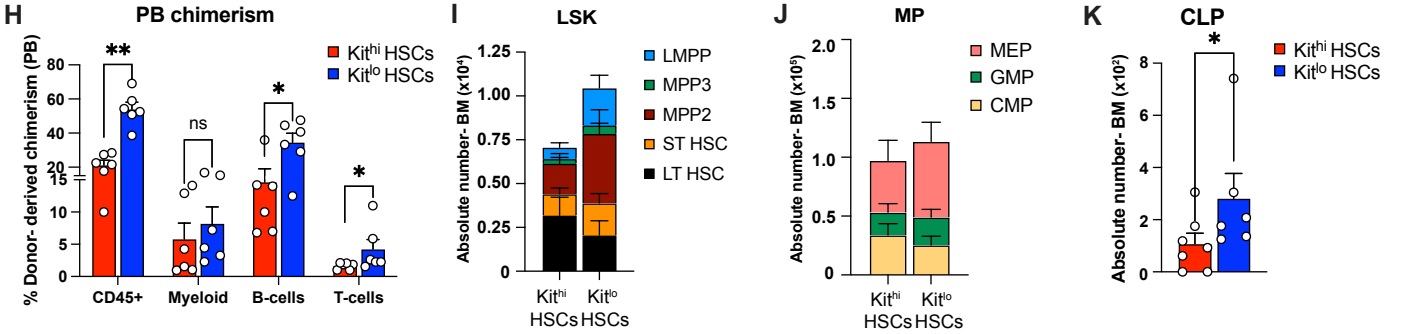

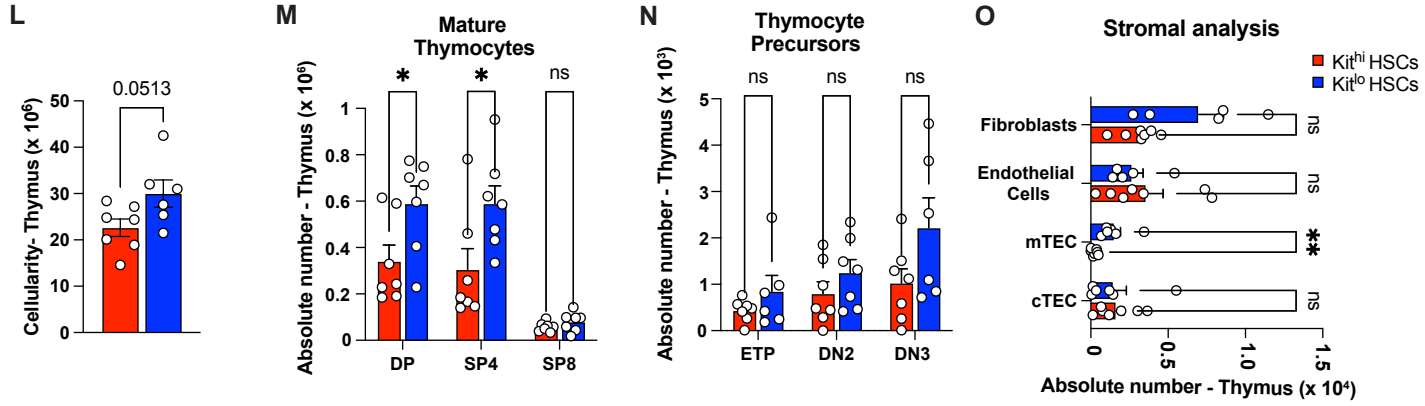

Figure S8

Equal Competition Tx

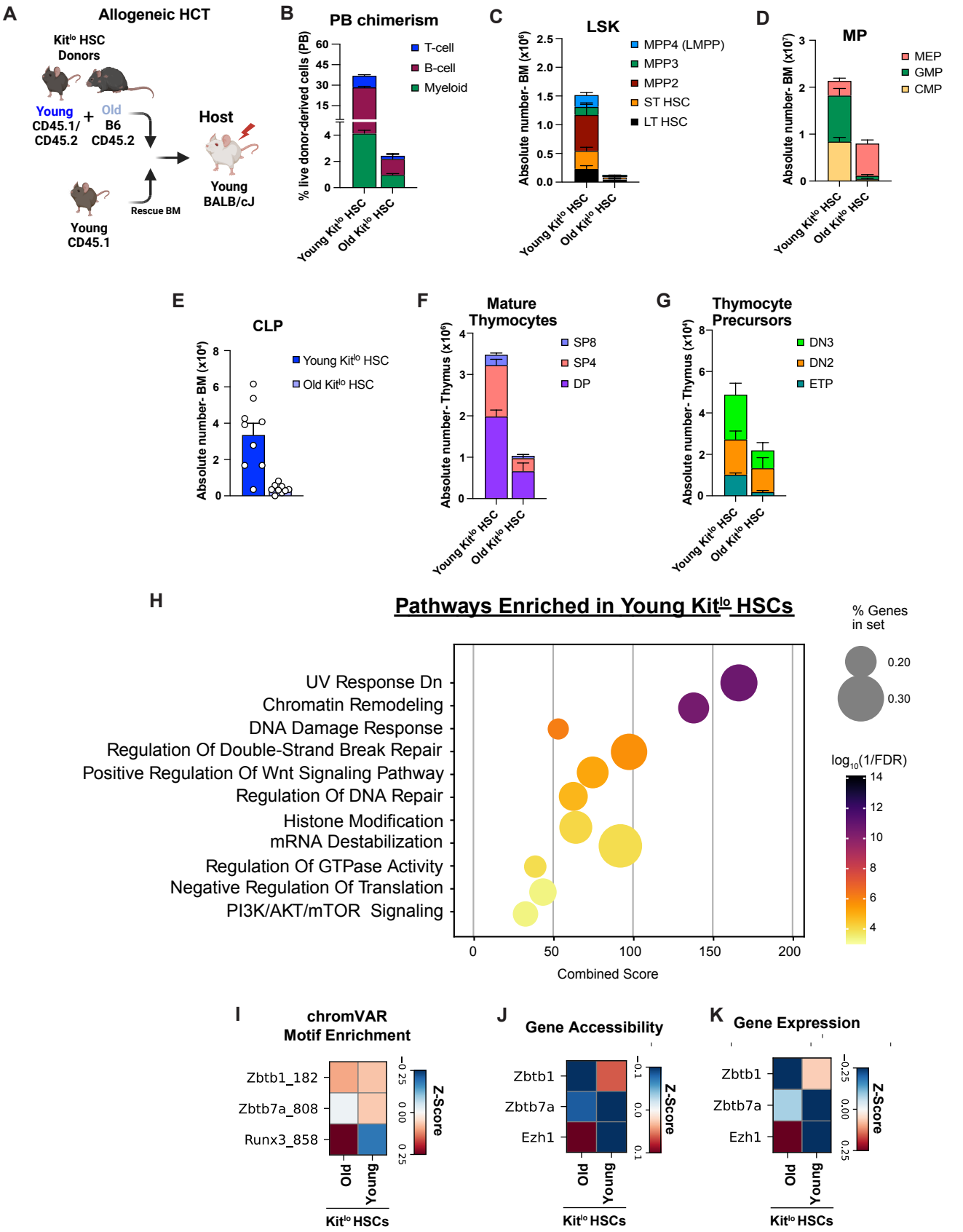

Figure S9

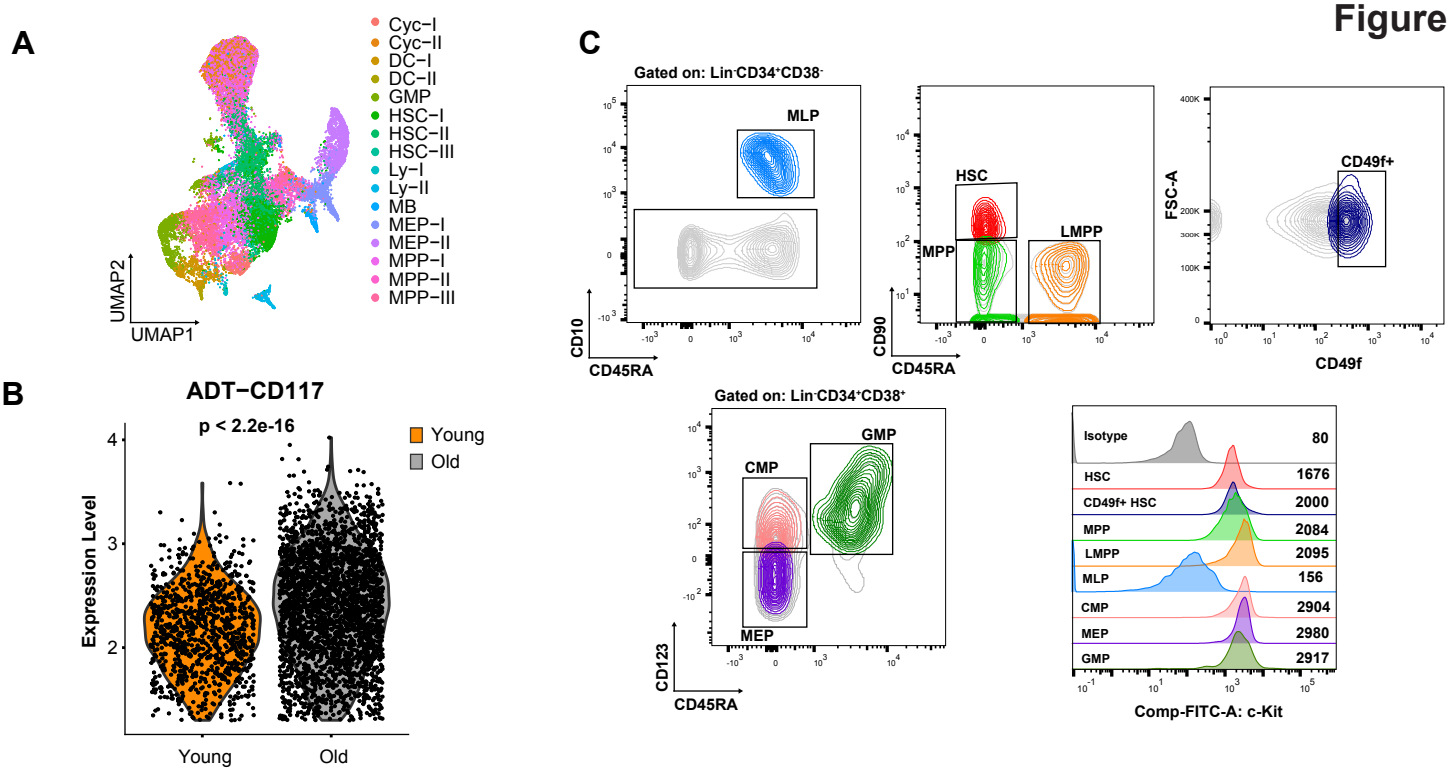
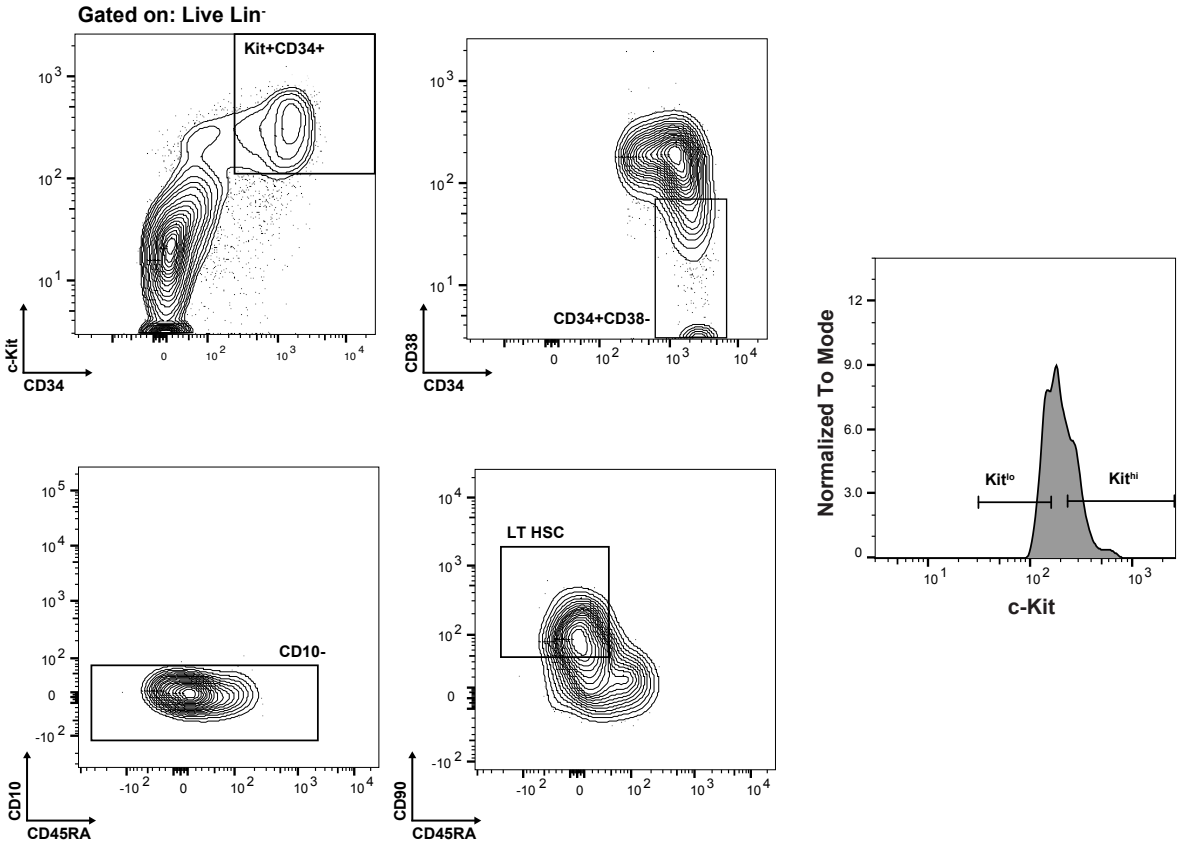
D Gating Strategy to Fractionate Kit Subsets in Human BM